The Cerithium limestone Member at Stevns Klint reflecting the carbonate production recovery after the K/Pg mass-extinction

Jacob Andersson

Dissertations in Geology at Lund University,
Master's thesis, no 692
(45 hp/ECTS credits)

Department of Geology
Lund University

2024

The Cerithium limestone Member at Stevns Klint reflecting the carbonate production recovery after the K/Pg mass-extinction

Master's thesis

Jacob Andersson

Department of Geology
Lund University
2024

Contents

Cover Picture: The Cerithium limestone and Fiskeler members at Kulstirenden locality (Stevns Klint, Denmark). Taken by Jacob Andersson.

The Cerithium limestone Member at Stevns Klint reflecting the carbonate production recovery after the K/Pg mass-extinction

Jacob Andersson

Andersson, J., 2024: The Cerithium limestone Member at Stevns Klint reflecting the carbonate production recovery after the K/Pg mass-extinction. *Dissertations in Geology at Lund University*, No. 692, 32 pp. 45 hp (45 ECTS credits) .

Abstract: The Cerithium limestone Member (Mb) at Stevns Klint holds an invaluable record in understanding the marine recovery after the K/Pg mass extinction. The Cerithium limestone Mb constitutes a pale yellow limestone including several different microfacies and a large boxwork of *Thalassinoides* burrows and flint nodules. This paper aims to describe these microfacies in detail and document their vertical and lateral distribution. To achieve these goals, two sites were sampled along the cliff of Stevns Klint, one at Kulstirenden locality and one at Rødvig. Twenty-eight thin sections were made from 16 samples from both sites; the thin sections were classified petrographically using Dunham classification. Representative samples were point-counted and further analyzed with SEM. Following the observations, the Cerithium limestone Mb was subdivided into subunits A-D with unit D being unique to Kulstirenden. Subunit A shows at both sites a bryozoan-dominated bioclastic rich wackestone/packstone associated with crinoids. The subunit B consists of a foraminiferal-dominated bioclastic-poor wackestone/mudstone with an increasing amount of sponge spicules up section. Subunit B at Kulstirenden contains more sponge spicules than at Rødvig and is more condensed. Subunit C shows a bioclastic-poor wackestone dominated by sponge spicules and calcispheres. Subunit D shows a mudstone with rare bioclasts dominated by echinoderm spines and foraminifera as well as a bioclastic-poor wackestone (15% bioclast content). As subunit D is unique to Kulstirenden and exists above the *Thalassinoides* marker horizon, it could represent strata missing at Rødvig. Such erosion is possibly marked by the hardground at the top of the Cerithium limestone Mb at both sites, which therefore may have some topographic relief. In some instances, bioturbation causes gradual but sometimes sharp boundaries between the microfacies, except for subunit A, which is consistent at both sites. The distribution of the microfacies from subunits B-D appears to show a slight increasing trend in bioclast content but is not significant enough to suggest a change in energy regime. On a microscale there are bioturbation traces separating the mud and wackestone. Because of this the Cerithium limestone Mb heterogeneity is probably not a change in energy regime but is more likely caused by extensive bioturbation. However, some thin-sections show varying degrees of sorting and fragmentation that could indicate that some level of sea-floor current transport did occur. More research is needed to clarify the lateral and vertical facies variation of the Cerithium limestone Mb at Stevns Klint.

Keywords: Bioturbation, Point-counting, Dunham classification, Bioclasts, Lithostratigraphy, Bryozoans, Foraminifera.

Supervisor(s): Sylvain Richoz, Mikael Calner

Subject: Sedimentary Geology

Jacob Andersson, Department of Geology, Lund University, Sölvegatan 12, SE-223 62 Lund, Sweden. E-mail: Jacob.985@hotmail.se.

Cerithiumkalkstenen vid Stevns Klint en återspegling av karbonatproduktionen återhämtning efter massutrotningen av K/Pg

Jacob Andersson

Andersson, J., 2024: Cerithiumkalkstenen vid Stevns Klint en återspegling av karbonatproduktionen återhämtning efter K/Pg massutdöendet. *Examensarbeten i geologi vid Lunds universitet*, Nr. 692, 32 sid. 45 hp.

Sammanfattning: Cerithium kalkstenen i Stevns Klint håller ett ovärderligt arkiv för att förstå den marina återhämtningen efter K/Pg massutdöendet. Cerithium kalkstenen är en blekgul kalksten uppbyggd av flera olika microfacies samt ett stort boxnätverk av *Thalassinoides*gångar och flint noduler. Denna avhandling syftar till att beskriva dessa microfacies i detalj samt dokumentera deras vertikala och laterala utsträckning. För att uppnå syftet togs prover från två lokaler längs med Stevns Klint, en nära Rødvig och en vid Kulstirenden. Tjugoåtta tunnslip gjordes från 16 prover från båda lokalerna; tunnslipen klassificerades petrografiskt med Dunhams klassifikation system. Representativa prover punkträknades och analyserades i mer detalj genom SEM analys. Efter utförda observationer uppdelades Cerithium Kalkstenen i flera subenheter A-D, där enhet D är unik till Kulstirenden. Subenhet A innehåller på båda lokalerna en bryozoan dominerande bioklastrik wackestone/packstone associerad med crionoider. Subenhet B början betecknas av en formanifera dominerande bioklast fattig wackestone/mudstone med ett successivt ökande antal av svampspiklar uppåt. Subenhet B vid Kulstirenden innehåller mer svampspiklar än Rødvig samt är mer koncentrerad. Subenhet C visar en bioklast fattig wackestone dominerad av svampspiklar och ”calcispheres”. Subenhet D visar en mudstone med sällsynta bioklaster dominerade av tagghudingar och foraminfera såväl som en bioklastfattig wackestone (15% bioklaster). Eftersom subenhet D är unik till Kulstirenden och återfinns ovanför *Thalassinoides* led horisonten, så kan enheter representera förlorad strat vid Rødvig lokalen. Sådan erosion markeras potentiellt av den erosionshårdbotten som finns ovan Cerithium kalkstenen. Därav kan den antas ha en viss topografisk relief. I vissa fall orsakar bioturbationen gradvisa övergångar men ibland skarpa gränser emellan mikrofacierna. Förutom subenhet A som är konsekvent över båda lokalerna. Distributionen av mikrofacies i subenhet B-D visar på en minimalt ökande trend i bioklastinnehåll men förändringen är inte signifikant nog att föreslå att ändringar i havsströms styrka har sket. På mikroskalan finns det en klar bioturbation som separerar mud och wackestone mikrofacierna. Således är det sannolikt att Cerithium kalkstenens heterogenitet inte beror på havsströmsändringar utan extensive bioturbation. Dock visar vissa tunnslip en viss fragmentering och sorterings grad vilket kan indikera att en viss transport över havsbotten fanns. Mer forskning behövs för att kunna klargöra de laterala och vertikala facies variationerna inom Cerithium Kalkstenen vid Stevns klint.

Nyckelord: Bioturnation, Punkträkning, Dunham klassifikation, Bioklaster, Lithostratigraphy, Bryozoa, Foraminfera.

Handledare: Sylvain Richoz, Mikael Calner

Ämnesinriktning: Sedimentär geologi

Jacob Andersson, Geologiska institutionen, Lunds Universitet, Sölvegatan 12, 223 62 Lund, Sverige. E-post: Jacob.985@hotmail.se.

1. Introduction

The K/Pg extinction event is one of the most profound extinction events in the Earth's history (D'Hondt et al., 2005; Alegret et al., 2012; Henehan et al., 2019). The extinction devastated many taxa with 75% of all marine life and 50% of all terrestrial life being extinguished (Alvares et al., 1980; Schulte et al., 2010). The cause of the extinction is believed to have been the Chicxulub asteroid impact in the Yucatan peninsula at 66.04 Ma (e.g. Alvarez et al., 1980; Shulte et al., 2010; Alegret et al 2012), vaporizing the target rock and leading to major carbonic gas and dust release causing devastating chain reactions. Some of the main drivers of the extinction have been suggested to be rapid ocean acidification, acid rain and global darkness (Shulte et al., 2010; Alegret et al., 2012; Henehan et al., 2019). However, there was already a weakening of the ecological system before the impact, caused by mass vulcanism related to the Deccan flood basalts, responsible for the late Maastrichtian thermal maximum (Hart et al., 2005; Henehan et al., 2019; Lowery et al., 2020). All these factors led to a weakening of the biological pump with a sharp reduction of pelagic calcifiers causing a devastating disruption throughout all marine trophic levels (Shulte et al., 2010; Alegret et al., 2012; Henehan et al., 2019; Bralower et al., 2020). Evidence for the Chixulub asteroid impact was recorded among others at the Fiskeler Member (Mb) extinction layer at Stevns Klint, Denmark by Alvarez et al. (1980). They noticed a sharp iridium anomaly in the Fiskeler Mb clay layer. Iridium is an element that only occurs in low concentrations on Earth. The Fiskeler Mb layer contained substantially higher concentrations of iridium leading them to conclude that an asteroid must have been responsible (Alvarez et al., 1980). Apart from recording the extinction level itself the succession at Stevns Klint is one of the first localities where the base of the Danian was set (Desor, 1847; Hart et al, 2005). It houses a nearly complete stratigraphical record covering the upper Maastrichtian – Paleogene of the Danish basin (Surlyk et al., 2006; Rosenkrantz et al., 2021). During the K/Pg extinction, Stevns Klint and the Danish basin were located at 45 degrees North (Bernecker & Weidlich, 2005). Stevns Klint at this time was deep marine cold-water carbonate environment situated on a continental shelf. It hosted a rich fauna consisting of solitary corals, bryozoans, brachiopods, echinoderms and mollusks making it ideal for studying marine environmental responses (Bernecker and Weidlich, 2005). Stevns Klint's relatively complete stratigraphy and carbonate lithology highlight it as an optimal place to study not only the extinction of marine fauna but also their subsequent recovery. After the Fiskeler Mb extinction layer was deposited, a 40cm -1 m thick limestone called the Cerithium limestone Mb was deposited. This thin limestone unit provides a record of the early carbonate production recovery just after the mass extinction (Rasmussen et al., 2005; Surlyk et al., 2006; Henehan et al., 2019). Even though Stevns Klint has been extensively studied, our understanding of the Cerithium limestone Mb remains lacking. While its stratigraphical extent and general formation are decently understood, its exact lithostratigraphic composition on the micro-scale is poorly studied. This leads to remaining questions about the depositional environment and marine carbonate recovery in the North Sea after the K/Pg extinction (Surlyk et al., 2005; Lykke-Andersen & Surlyk, 2004; Störling et al., 2024). The Cerithium limestone Mb was thought to be a lithological homogenous unit but recently, Störling et al. (2024) showed that this was not the case. Moreover, the Cerithium limestone Mb is a stratigraphical unit whose thickness and chronostratigraphic extent vary across different localities along the Stevns Klint cliffs due to the prominent Cretaceous mound structure, shaping the paleobathymetry of the region and in turn influencing the spatial extent of Cerithium limestone (Surlyk et al., 2006; Anderskouv et al., 2007). This has caused the lateral and vertical extent of these microfacies to remain poorly understood (Störling et al. 2024).

In this thesis, I aim to add to the data collected by Störling et al. (2024) by studying the lateral and vertical variability of the microfacies in the Cerithium limestone. This will in turn increase our understanding of the petrography of the Cerithium limestone and in turn its depositional environment and the way of recovery of carbonate production after the K/Pg mass extinction. Some of the data collected during this study at Rødvig (vertical variability, point-counting) have been published in Störling et al. (2024).

My master thesis aims to:

- Petrographically characterize, through thin-section observation, the Cerithium limestone Mb at two localities along Stevns Klint, separated by 19 km.
- Quantify through point-counting the different components of each microfacies.
- Understand the different generations of burrows and their relation to the microfacies.
- Document and compare any lateral changes in the microfacies.
- Address the evolution of the depositional environment for the Cerithium limestone Mb.

2. Geological setting and stratigraphy

Stevns Klint is a 14.5 km long and up to 41 m high coastal cliff south of Copenhagen in Denmark (Fig. 1) (Rosenkrantz et al., 2021). The long cliff section exposes the upper Maastrichtian and lower Danian and represents the eastern preserved parts of the Danish basin. Stevns Klint is a unique locality in the world as it shows an almost complete cycle of a cold-water carbonate environment responding to an extinction event from its stop in carbonate production to its recovery. Stevns Klint contains the famous iridium anomaly at the K/Pg boundary (Alvarez et al., 1980; Hart et al., 2005; Rosenkrantz et al., 2021)

2.1 Danish basin

The Danish basin is an early Permian to Cenozoic intracratonic basin located in the present-day North Sea.

The basin borders are loosely defined but are located between the Danish Central Graben in the west, the Ringkøbing–Fyn High in the South, and the Fennoscandian shield in the North (Fig. 2) (Vajbeck, 1989; Nielsen, 2003; Møller & Rasmussen, 2003).

The tectonic development of the Danish basin started in the early Permian with extension faulting linked to the breakup of Pangea (Andersen et al., 1982; Nielsen, 2003). Rifting in the North Sea caused a triple junction creating several graben structures like the Oslo and Central Graben. The Central Graben reaches 500 km in an NNW-SSE direction. The Danish Central Graben is located east to southeast of the Central Graben and includes the Danish basin in the southeast (Andersen et al., 1982; Vejbaek, 1989; Nielsen, 2003; Patruno et al., 2022). The basin development from the Permian to the earliest Triassic is summarized by extensional faulting and subsidence due to thermal cooling along with a crustal density increase (Vejbaek, 1989; Nielsen, 2003). During the late Permian, a large thickness of evaporites was deposited in the Danish basin, these later became responsible for halo-kinetic movements that occurred from the Late Triassic to the Cenozoic (Sørensen, 1982). During the Early and Middle Triassic, the area was hot and arid promoting the deposition of many terrestrial siliciclastic rocks like arkose sandstones across the basin (Nielsen, 2003).

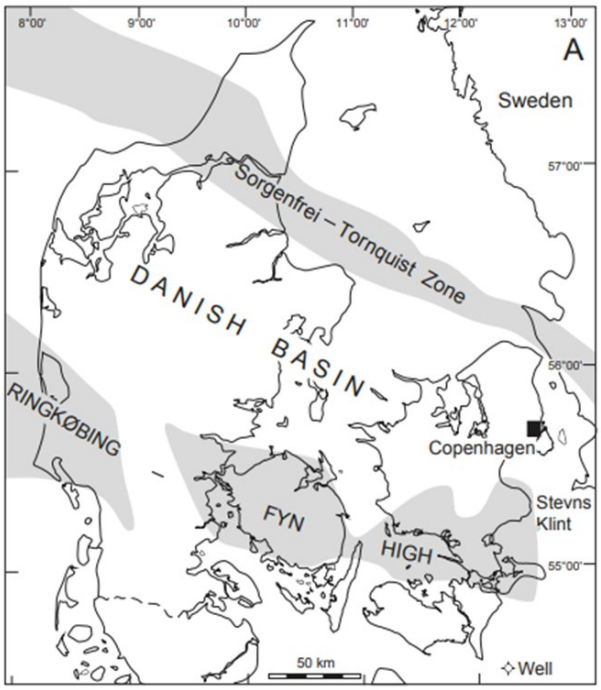

Fig. 2: Map showing the major structural elements of the Danish basin. Originally from Surlyk (2006) and modified by Rosenkrantz et al. (2021).

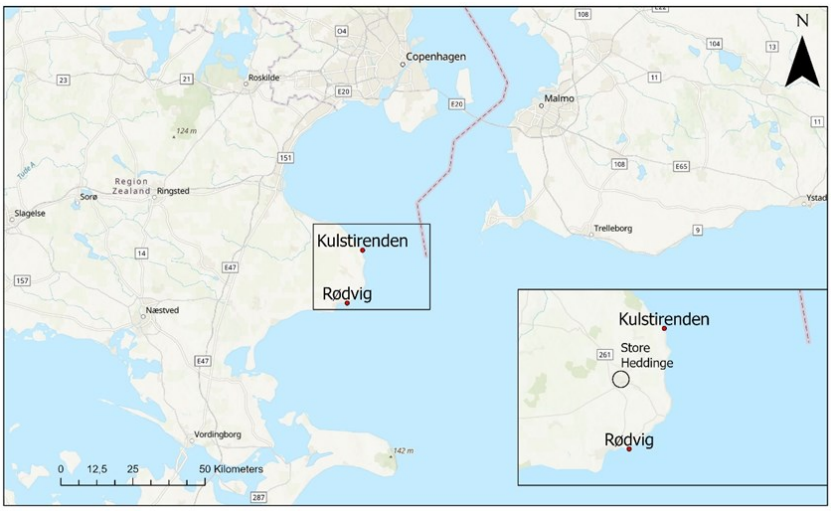

Fig. 1: Overview map of the study area at Stevns Klint with the two sample sites used in the study, located at Rødvig and Kulstirenden. Background ArcGIS pro base map, map sources: Esri, CGIAR, N Robinson, NCEAS, USGS; Tom Tom, Garmin, Foursquare, FAO, METI/NASA, USGS; Esri, CGIAR, Geodatastyrelsen, N Robinson, NCEAS, USGS.

The Upper Triassic-Jurassic part of the Danish basin is a 1 km thick succession consisting of mainly Norian deposits (Nielsen, 2003). The lithologies of this period are split between either clay or marl, fossil-rich and oolitic limestone that were deposited in the central parts of the basin. Siliciclastic deposition during the Rhaetian- Hettangian did occur with large amounts of mainly fluvial, offshore and shoreface sediments (Nielsen, 2003). These siliciclastic sediments form some of the thickest sandstone formations near the eastern and southern basin margins (Nielsen, 2003). The Late Triassic – Jurassic was a period of low tectonic activity mainly with extension leading to a gradual deepening of the basin with mainly marine deposits until the Middle Jurassic (Neilsen, 2003). In the Middle Jurassic, new rifting in the North Sea caused the region to experience a central uplift, eroding the Lower Jurassic sediments on the Ringkøbing–Fyn High (Nielsen, 2003; Surlyk et al., 2003). In the Middle-Late Jurassic the basin experienced gradual subsidence and expansion (Nielsen, 2003). The basin during this time was characterized by a sea level rise with large mud deposits mixed with braided fluvial and lagoonal sediments (Nielsen, 2003; Møller & Rasmussen, 2003). The Lower Cretaceous stratigraphy of the Danish basin consists of marine clays and bioturbated marlstone that gradually transitioned into the massive Chalk Group in the early Cenomanian (Ineson et al., 2022). The Jurassic – Lower Cretaceous strata are disrupted by salt diapirs and other halokinetic movements (Sørensen, 1982; Møller & Rasmussen, 2003; Nielsen, 2003).

In the Cretaceous, the extension of the Danish basin stopped, and the basin only experienced further thermal subsidence until the Late Cretaceous (Andersen, 1982). Subsidence coupled with global sea level rise, warm and humid climate caused the deposition of transgressive sediments in the Early Cretaceous and large amounts of marine chalk in the Late Cretaceous- earliest Palaeocene (Andersen, 1982; Surlyk et al., 2003; Boussaha, 2017). During the Paleogene, tectonic activity resumed with the basin experiencing around 600 m of uplift due to basin inversion caused

by alpine movement (Hansen et al., 2021). The uplift lasted until the end of the Neogene (Andersen, 1982; Bernecker & Weidlich, 2005). Depositions during the early Cenozoic consisted mainly of clay sand and siltstone (Andersen, 1982). During the mid-late Cenozoic, the basin experienced only minor tectonic activity and some halokinetic movement. Much of the Cenozoic sediments as well as some parts of the upper Danian succession were eroded during the Neogene uplift (Nielsen et al., 2011). Further, quaternary glaciations caused the reburial of Cretaceous and Paleogene chalk deposits making the Chalk group succession not entirely visible in the current day (Nielsen et al., 2011).

2.2 Stevns Klint stratigraphy

The stratigraphy of Stevns Klint includes the widespread Chalk Group, including the upper Maastrichtian -lower Danian (Surlyk et al., 2003, 2006; Rosenkrantz et al., 2021). The lowermost exposed part of the Chalk Group at this locality is the Maastrichtian coccolith-rich white chalk which is part of the Møns Klint Formation (Fm) and houses the Sigerslev and Højerup members (Mb) (Fig. 3) (Surlyk et al., 2006; Rosenkrantz et al., 2021). The chalk is overlain by the Rødvig Fm, which contains the famous clay marl layer of the Fiskeler Mb and the Cerithium limestone Mb (Fig. 3). The uppermost part of the Chalk Group is the Korsnæb Mb, the lowermost member of the Stevns Klint Fm. It comprises the lower Danian bryozoan mounds (Fig. 3) (Surlyk et al., 2006; Rosenkrantz et al.,2021).

The lowest and oldest layer at Stevns Klint is the Sigerslev Mb part of the Møns Klint Fm. The Møns Klint Fm was referred to as Tor Fm in older literature (Surlyk et al 2006; Rosenkrantz et al. 2021). The Sigerslev Mb contains an upper Maastrichtian wackestone with a coccolith-rich matrix. The unit has a maximum thickness of 30 m in outcrop, but seismic data suggest that it reaches up to 70 m, of which the bulk is below sea level (Hart et al., 2005; Rosenkrantz et al., 2021). The lower outcropping part of the Sigerslev Mb contains bryozoan-rich mounds that gradually transition upwards into a benthic fossil-poor gentle wavy bedding structure geometrically similar to mounds. The mound structures are not true biological mounds as they do not show typical biogenic carbonate build-up and have generally low amplitudes (Hart et al., 2005; Surlyk et al., 2006; Rosenkrantz et al., 2021). The upper part of the Sigerslev Mb is also a coccolith chalk and has the same petrology as its lower counterpart but contains a low number of benthic fossils and has an abundance of flint nodules throughout (Surlyk et al., 2006; Surlyk & Lykke-Andersen, 2007; Rosenkrantz et al., 2021). The transition into a more horizontally bedded chalk in the lower middle part of the Sigerslev Mb (Fig. 4) has been interpreted as reflecting a transition into a deeper marine low-energy environment (Surlyk et al., 2006). The wavy structure is thought to be caused by the accumulation of fine-grained suspended chalk material settling amongst low -velocity currents (Anderskouv et al., 2007). These low-velocity currents are believed to be formed by a system of WNW-ESE orientated valleys (Lykke-Andersen & Surlyk, 2004; Anderskouv et al., 2007).

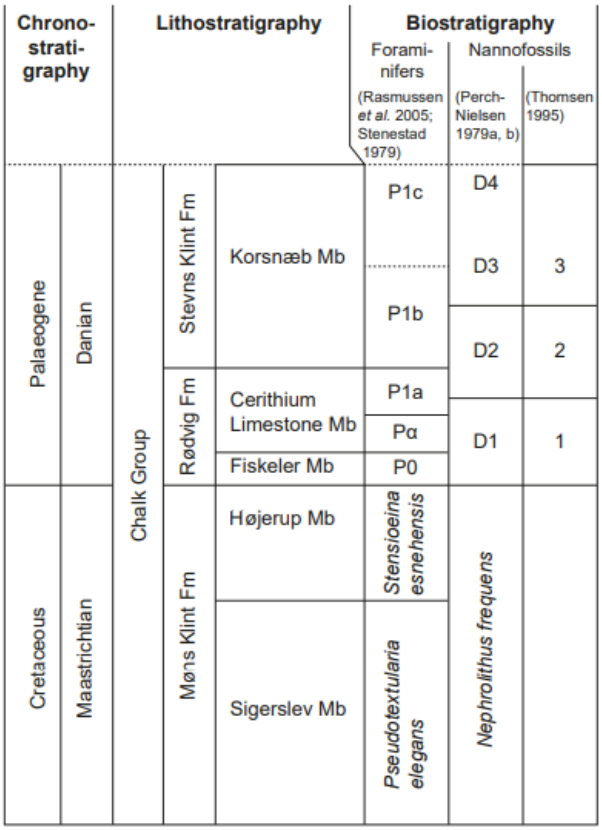

Fig. 3: A schematic of the chrono-, litho-, and biostratigraphy at Stevns Klint coastal cliff south of Copenhagen in Denmark. The figure covers the Upper Cretaceous Sigerslev Mb to the Danian Korsnæb Mb. The biostratigraphy is compiled from Rasmussen et al. (2005), Perch-Nielsen (1979) and Thomsen (1995). The Figure was taken from Rosenkrantz et al. (2021).

The mounds at Stevns Klint align with the paleocurrents evidenced by paleo-bathymetry analysis of the Kattegat Sea floor showing that the paleo current in the area flowed in a WNW-ESE bound direction in the late Maastrichtian (Lykke-Andersen & Surlyk, 2004; Surlyk et al., 2006). Conversely, seismic analysis of the area showed that many of the other mound formations at Stevns Klint followed the WNW-ESE going currents during their formation (Lykke-Andersen & Surlyk, 2004; Surlyk et al., 2006). The top of the Sigerslev Mb is occasionally marked by twin-bedded hardground marking a period of total stop in sedimentation followed by *Thalassinoides* burrowing. *Thalassinoides* is a trace fossil believed to be formed by a crustacean making box works of burrows which are preserved during periods of low sedimentation rate (Myrows, 1995). These burrows are often silicified during digenesis into flint nodules (Surlyk, 1995; Myrow, 1995). *Thalassinoides* is often used as a marker bed at Steven Klint as it can often be linked to burrow 30-50 cm consistently below multiple hardgrounds (Surlyk et al., 2006). These prominent flint bands are often used as a marker bed for the end of the Sigerslev Mb and the start of the Højerup Mb (Surlyk et al. 2006; Surlyk & Lykke-Andersen., 2007; Rosenkrantz et al. 2021).The Højerup Member is the next member in the Møns Klint Formation, the member is a 4-5 m

bryozoan-mounded wackestone (Surlyk et al., 2006; Rosenkrantz et al., 2021).

The Højerup member is in older literature referred to as the "Gray chalk" due to its apparition sometimes in a gray stained coloration at Stevns Klint. (Rosenkrantz, 1937; Surlyk et al., 2006). The Højerup Mb is often distinguishable in the field by a distinct boxwork of *Thalassinoides* burrows in its upper part. The Højerup Mb thins out towards the north along Stevns Klint coastline and is only 1 m thick at Kulstirenden (Rosenkrantz et al., 2021).

The Højerup Mb transitions abruptly into the Fiskeler Mb of the Rødvig Fm. This boundary and thin bed marks the mass extinction level and the start of the Danian Stage. The Fiskeler Mb starts at the base with a very thin Fe-stained marl with dissolved clay wisps and transitions into a silt-clay layer with pyrite (Surlyk et al., 2006; Hart et al., 2005; Rosenkrantz et al., 2021). The Fiskeler Mb is commonly 5-10 cm thick but reaches a thickness of ca 30 cm at Kulstirenden (Rosenkrantz et al., 2021; Surlyk et al., 2006). The Fiskeler Mb clay has at its base a sublayer of black clay where the world-famous iridium anomaly was detected (Alvarez et al., 1980). Because of the Højerup Mb mound structures the Fiskeler Mb thickness varies greatly as it is confined to low-relief depressions between the crests of the Maastrichtian Højerup Mb mounds (Fig. 4) (Rosenkrantz et al., 2021; Surlyk et al., 2006). A profile from Rosenkrantz et al. (2021) showed that there are in total 13 such depressions where the Fiskeler Mb is preserved. The Fiskeler Mb is deposited in a marine environment as indicated by the presence of a marine planktonic foraminiferal fauna (Hart et al., 2005). The upper boundary of the Fiskeler Mb can be either gradual or sharp as it passes upwards into the overlaying Cerithium limestone Mb (Rosenkrantz et al., 2021).

The Cerithium limestone Mb represents the bulk and upper part of the Rødvig Fm and is a partially cemented limestone of earliest Danian age (Fig. 3) (Hart et al., 2005; Surlyk et al., 2006; Rosenkrantz et al., 2021). It shows wavy fold-like structures interpreted to be caused by the paleo-bathymetry at the time of deposition (Rosenkrantz et al., 2021). The limestone normally varies in thickness between 30-60 cm, but is sometimes thinner or cut out, whereas it reaches a maximum thickness of 120 cm at Kulstirenden (Rosenkrantz et al., 2021; Hart et al., 2005; Surlyk., et al 2006). Hence, because of the uneven paleobathymetry, the Fiskeler Mb and Cerithium Mb are discontinuous in the northern areas of Stevns Klint, for example at the Korsnæb cliff. The Cerithium limestone Mb has also been suggested to be diachronous due to the basal part of the Cerithium limestone Mb being younger towards the north (Rasmussen et al., 2005). However, this is debated (e.g. Störling et al., 2024). The thickness variance is further complicated as the top of the Cerithium limestone Mb is marked by an erosional hardground that truncates the unit and in some places the Maastrichtian mounds from the Højerup Mb (Surlyk et al., 2006; Rosenkrantz et al., 2021). Because of the multitude of mound structures controlling the stratal positions, the position of the hardground varies from ca 5 m below present-day sea level to ca 30 m above. Due to the mounds causing the height differences, the hardground can sometimes

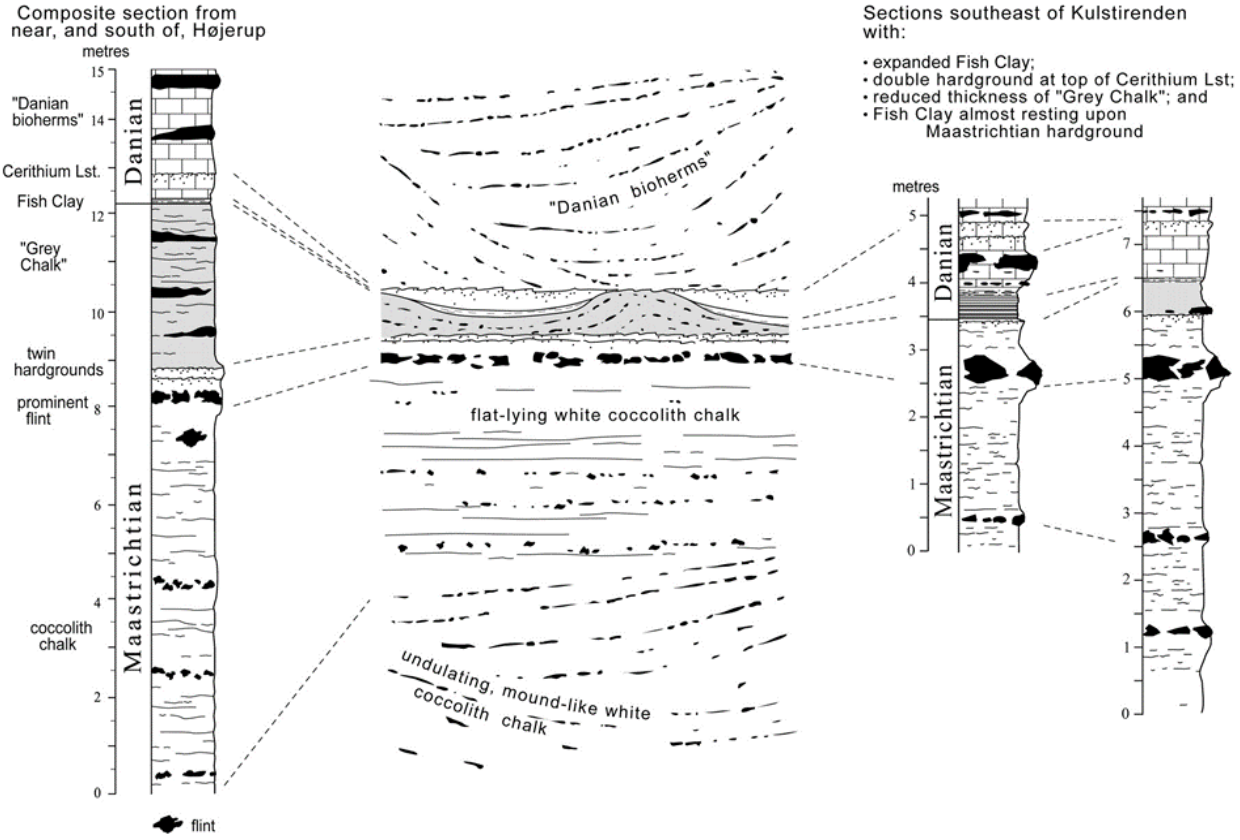

Fig. 4: Stratigraphic log over Stevns Klint comparing two different localities near Højerup and Kulstirenden, respectively. Note the lithostratigrphic variation within the different units. From Hart et al. (2004).

curve in either an anticline or syncline-like manner. The area below the hardground is more cemented as well as showing a dense network of *Thalassinoides* burrows (Surlyk et al., 2006). The *Thalassinoides* burrows were formed due to the reprecipitation of silica gathering in nodules left by the burrowing (Hart et al., 2005). *Thalassinoides* has been found to burrow to a consistent depth of 30 cm below the hardground. At Kulstirenden, the Cerithium limestone Mb has developed a twin hardground structure, i.e. two hardgrounds occurring in a short distance from each other, like the double hardgrounds at the top of the Sigerslev Mb (Fig. 4) (Surlyk et al., 2006). The Cerithium limestone Mb contains an abundance of *Thalassinoides* burrows that contain reworked sediment from the overlaying Danian bryozoan mounds (Surlyk et al., 2006; Hart et al., 2006; Rosenkrantz et al., 2021). The lithology of the Cerithium limestone Mb is debated, it has been described as a micritic limestone containing either an abundance or lack of fossils (Hart et al., 2005; Surlyk et al., 2006; Störling et al., 2024). The Cerithium limestone Mb has been shown to have a big variation in different fossil assemblages. For example, it contains high diversity planktonic foraminifers mostly dominated by *Heterohelix* spp. but with a higher abundance of *Globoconusa daubjergensis* in some localities (Rasmussen et al., 2005). The foraminiferal assemblage is also very fragmented causing difficulties in genus identification (Hart et al., 2005; Rasmussen et al.,2005). The recent study by Störling et al. (2024) suggested that another reason for the variation in foraminiferal fossil findings could be due to the degree of diagenetic dissolution of foraminiferal shells varying very locally. There is also evidence pointing to the occurrences of ammonites post K/Pg extinction in the Cerithium limestone Mb (Machalski, & Heinberg, 2005).

Overlaying the Cerithium limestone Mb is the Korsnæb Mb which marks the start of the Stevns Klint Formation (Fig. 3) (Hart et al., 2005; Surlyk et al., 2006; Rosenkrantz et al., 2021). The Korsnæb Mb is a Danian bryozoan rudstone to packstone containing large mounding bioherms (Hart et al., 2005; Surlyk et al., 2006; Rosenkrantz et al., 2021). The visible thickness of the Korsnæb Mb at Stevns Klint is around 20 m but the top half of it is not exposed at Stevns Klint. In full, the member is around 50 m in thickness (Thomsen 1995; Surlyk et al., 2006). These mounds could form due to an increase in accommodation space during the earliest-middle Danian (Surlyk et al., 2006). The bryozoan mounds are of a biogenic origin and consist of a mud matrix with millimeter-scale skeletal fragments of corals and bryozoans. The mound's petrology is heterogenous with the southern flanks typically developed as either rudstones or floatstones, whereas the northern flanks consist mainly of packstones (Surlyk et al., 2006) The Korsnæb mounds build in an SSW direction where the axis from the mound crests points in a WNE-ESE direction. The mound axis is parallel with the paleo-bathymetry structures in the Højerup Mb and the paleocurrent in the area (Surlyk et al., 2006; Lykke-Andersen & Surlyk, 2004).

2.2.1 Lithostratigraphy of the Rødvig locality, southern Stevns Klint

The studied Rødvig section is located on the coast at the southern end of Stevns Klint ca 1300 m east of Rødvig harbour and is the type locality for the Rødvig Fm (Surlyk et al., 2006; Rosenkrantz et al., 2021). The locality covers a time period from the uppermost Maastrichtian- Paleogene (Surlyk et al., 2006; Rosenkrantz et al., 2021). Apart from the Rødvig Fm, the Rødvig locality houses the upper Maastrichtian Højerup Mb as well as the lower part of the Korsnæb Mb (Fig. 5) (Surlyk et al., 2006; Rosenkrantz et al., 2021). The Rødvig Fm is around 30-70 cm in thickness at Rødvig but up to 80 cm further northeast of the locality (Surlyk et al., 2006;). The Fiskeler Mb is discontinuous in most of Stevns Klint, but it has its longest extent laterally at Rødvig where it has a thickness of around 5-10 cm (Surlyk et al., 2006). The Fiskeler Mb gradually transitions into the Cerithium limestone Mb at Rødvig. The Cerithium limestone Mb at Rødvig varies in thickness, the average thickness is around 25-40 cm thick. At Rødvig, mainly the lower- middle part of the Cerithium limestone Mb is visible (Surlyk et al., 2006). The limited thickness of the Cerithium limestone at Rødvig is due to the lower Danian erosional hardground that truncates the layer (Surlyk et al., 2006; Rosenkrantz et al., 2021). The hardground is located around 3-5 m above sea level and follows the paleo-bathymetry of the Maastrichtian mounds (Surlyk et al., 2006). Just below this hard ground at the top of the Cerithium limestone the prominent flint band of *Thalassinoides* burrows is visible and marks the top of the Cerithium limestone Mb at Rødvig (Surlyk et al., 2006; Rosenkrantz et al., 2021). Overlaying the Cerithium limestone Mb at Rødvig is the Korsnæb Mb showing thick Danian bryozoan mounds with alternating flint bands in the mound layers (Surlyk et al., 2006).

2.2.2 Lithostratigraphy of Kulstirenden, northern Stevns Klint

Kulstirenden is a coastal cliff located at the northernmost part of the Stevns Klint succession south of Præsteskov (Surlyk et al., 2006). The stratigraphy of Kulstirenden covers the upper Maastrichtian Sigerslev Mb with wavy gentle mounding to the lower Danian part of the Korsnæb Mb (Fig. 6) (Surlyk et al., 2006; Rosenkrantz et al., 2021). At Kulstirenden, mainly upper Maastrichtian chalk of the Sigerslev Member is exposed while the Højerup Mb has almost completely thinned out. The Sigerslev unit at Kulstirenden is about 10 m thick (Surlyk et al., 2006). In the northern end of the Kulstirenden cliff, there are elevated outcrops of the Rødvig Fm with thick sections of both the Cerithium limestone and Fiskeler Mb (Surlyk et al., 2006). At Kulstirenden, the Rødvig Fm has its biggest vertical extent with the Fiskeler Mb reaching a thickness of 30 cm and the Cerithium limestone Mb reaching up to 120 cm (Surlyk et al., 2006). The extent of the layers varies laterally due to the mounds. At Kulstirenden, less of the Cerithium limestone Mb is visible compared to the outcrops in the Rødvig succession. At Kulstirenden the base of the unit is condensed or missing but instead, the top of the Cerithium lime-

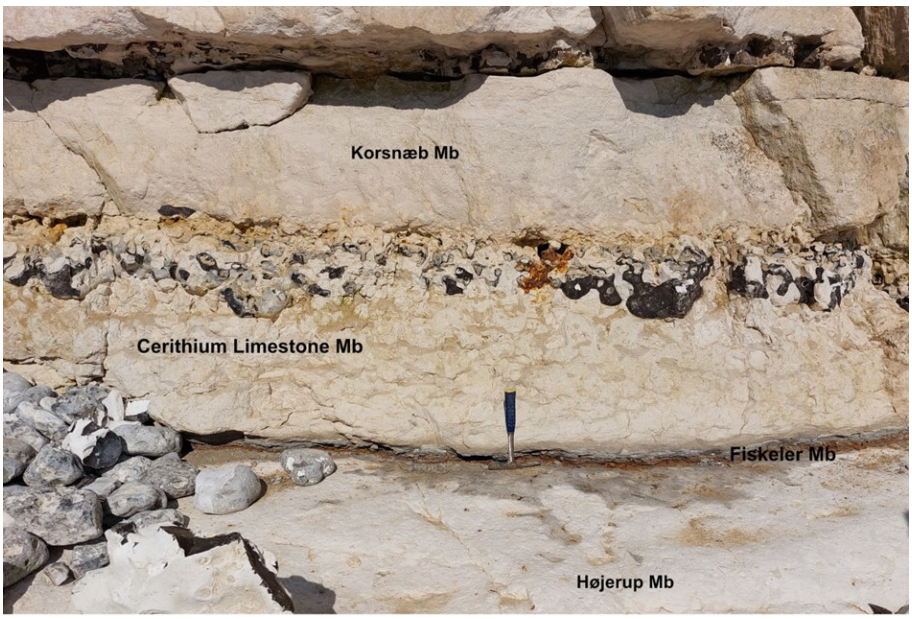

Fig. 5: Photo showing sample-site at the Rødvig locality, just north-east of Rødvig, showing the Cerithium limestone Mb and enclosing units.

Fig. 6: Overview photograph of the sampling site at Kulstirenden.

stone Mb is thicker (Surlyk et al., 2006; Rosenkrantz et al., 2021).

2.3 Marine evolution through the K/Pg interval at Stevns Klint

In this chapter, I review shortly the biostratigraphy of the succession and highlight the major changes during the mass-extinction and the different phases of the recovery.

2.3.1 Biostratigraphy of the Rødvig Fm at Stevns Klint

The biostratigraphy of the Fiskeler and Cerithium limestone members has been described in different ways throughout the years (e.g. Perch-Nielsen 1979; Thomsen 1995; Stansted 1997; Rasmussen et al., 2005). Early works mainly used echinoderms and macrofossils as a basis for division (Perch-Nielsen, 1979; Rasmussen et al., 2005). In more recent works, biostratigraphical divisions are made by using foraminiferal assemblages or calcareous nanoplankton (Rasmussen et al. 2005; Leighton et al., 2011). The latest foraminifera-based subdivision of the Rødvig Fm at Stevns Klint was done by Rasmussen et al. (2005) in which they subdivided the Rødvig Fm members into three zones, as seen in Figure 3. The P0 zone is based on the last appearance datum (LAD) of three Cretaceous taxa (*Rugoglobigerina, Globotruncana* and *Globigerinelloides)* and the first appearance datum (FAD) of a lower Danian taxon (*Vularugoglobigerina eugubina)* (Berggren and Miller, 1988; Rassmussen et al., 2005). The Pα is defined from the FAD of *Parvularugoglobigerina eugubina* to the FAD of *Parasubbotina pseudobulloides* sensu stricto. P1a zone is a subzone of P1 and is confined from the FAD of *Parasubbotina pseudobulloides* to the FAD of *Subbotina triloculinoides.* The P1a zone has been shown to thin out towards the northwest and was one of the arguments for the Cerithium limestone Mb as being diachronous (Rassmussen et al., 2005). Important to note is that the foraminiferal assemblages of the Cerithium limestone and Fiskeler members are potentially incomplete due to some potential shells dissolution during diagenesis (Hart et al., 2005). Because of this, there have been attempts to use dinoflagellate cysts for the biostratigraphy of these sections (Leighton et al., 2011). However, so far only marker specimens have been suggested and no full biozonation exists for Stevns Klint (Leighton et al., 2011). Other nannofossils zones have been established over the K/Pg extinction boundary at Stevns Klint. However, the resolution of these zones is less compared to foraminifera biostratigraphy (Perch-Nilesen, 1979; Thomsen, 1995; Surlyk, 2006).

One frequently used biozonation for the lower Da-

nian at Stevns Klint is based on planktonic calcareous nannofossils (Perch-Nielsen 1979) (Fig. 3). Since the Cerithium limestone Mb was deposited in a temperate area of the North Sea, Perch-Nielsen (1979) developed a biozonation based on a previously established zonation for the lower Danian from the northern Tethys Ocean. The Stevns Klint zonation uses subunits of the NP1 *Markalius inversus* zone (Martini, 1971). The lower Danian is comprised of the first two NP1 subzones D1 and D2. D1 is a zone bracketed between the LAD of *Biontholithus sporsus* and the FAD of *Zygodiscus sigmoides*, while D2 is bracketed between the FAD of *Zygodiscus sigmoides* and the FAD of *Cruciplocolithus tenuis* (Perch-Nielsen, 1979). Later, Thomsen (1995) updated Perch-Nielsens' biozonation (Fig. 3) and Burnett (1996) proposed an alternative one. Unlike Perch-Nielsen (1979), Burnett (1996) based his zonation on deep sea drill cores of the boreal regions around the North Sea (Burnett, 1996; Thibault et al., 2012). For this paper the zonation made by Perch-Nielsen (1979) will be used as it is the most common zonation used for Stevns Klint (i.e. Rasmussen et al., 2005; Surlyk et al., 2006; Rosenkrantz et al., 2021).

2.3.2 Marine faunal changes across the K/Pg boundary

During the K/Pg extinction interval, the marine organisms at Stevns Klint went through drastic changes. Coccolithophorids, the main pelagic calcifiers, were hardly hit and show a drastic decrease in diversity and abundance. They were replaced by a disaster taxon of dinoflagellate cysts and later by diatoms (Alegret et al., 2012; Lowley et al., 2019). Many groups such as bivalves, planktonic foraminifera, radiolarians, gastropods and bryozoans followed the expected trend during a mass-extinction. This trend starts with a sharp reduction in species abundance and diversity, abruptly followed by a high abundance and low diversity organisms i.e. single or few species dominating. The curve then stabilises to an equilibrium with increased diversification at the cost of abundance (Heinberg, 2005; Bernecker and Weidlich, 2005; Hansen and Surlyk, 2014). However, benthic groups were affected to varying degrees of severity (Heinberg 1999; Alegret et al., 2012). Some benthic groups such as benthic foraminifera and ostracods show a very minor reduction indicating that they might have been hit less than previously thought (Hart et al., 2005; Alegret et al., 2012). In the late Maastrichtian, the benthic fauna were dominated by a high diversity of bryozoan with a low abundance of Azooxanthellate corals (Bernecker and Weidlich, 2005). The bryozoan community remained relatively unchanged except for a sharp reduction in the earliest Danian eventually recovering in the middle Danian (Heinberg, 1999; Bernecker & Weidlich, 2005). The corals only underwent minor changes over the K/Pg (Bernecker & Weidlich, 2005). The late Maastrichtian shows the appearance of rare solitary communities of scleractinian corals and octocorals. Octocorals were found in the Cerithium limestone Mb and only a few solitary scleractinian coral species have been found in the Danish basin from the earliest Danian (Bernecker & Weidlich, 2005). The coral fauna would start to change later in the middle Danian where scleractinian corals started to be one of the main mound-building organisms (Bernecker & Weidlich, 2005; Hansen & Surlyk, 2014). The infaunal species at Stevns Klint, particularly the bivalves, show a high species abundance in the Maastrichtian followed by a sharp reduction during the extinction (Heinberg, 2005). However, extinction of bivalves in the chalk group is of a lower severity compared other formations globally. The bivalves show a quick recovery starting with the complete dominance of a single disaster species in the lowermost Cerithium limestone Mb P1a zone but later the bivalves quickly diversify, and the numbers of species evens out (Heinberg, 2005). The Cerithium limestone Mb is surprisingly diverse and consists of sponge, ostracods, bivalves, scaphopods, bryozoans, gastropods, pelagic and benthic foraminifera and solitary corals (Heinberg, 2005; Bernecker & Weidlich, 2005; Hansen & Surlyk, 2014).

2.3.3 Recovery from the K/Pg mass extinction as recorded in the Cerithium limestone Mb

The K/Pg extinction show good correlation to the Chicxulub impact, but the simultaneous eruption and formation of the Deccan traps did play a still discussed role (e.g Henehan et al., 2019). The Chicxulub impact caused a major release of greenhouse gases, sulfur and soot that was launched into the atmosphere (D'Hont et al., 2005; Schulte et al., 2010; Lowley et al., 2020). These factors led to major marine and atmospheric changes, most notably rapid ocean acidification, acid rain, and sunlight reduction. These factors lead to a collapse in photosynthesizing organisms, weakening the primary production and causing a cascading effect throughout all trophic levels (D'Hont et al., 2005; Schulte et al., 2010; Lowley et al., 2020). Rapid ocean acidification alongside hypoxia and near collapse of open ocean mixing during the K/Pg caused major stress on the pelagic groups (Lowley et al., 2020), contributing to the fact that 90% of the pelagic calcifiers such as nanoplankton and pelagic foraminifera went extinct. This disrupted the marine ecosystem and geochemical cycles (e.g. Alegret et al., 2012; Henehan et al., 2019; Lowley et al., 2020). In the aftermath, the pelagic calcifiers were replaced by silicifying planktons like radiolarians and diatoms which greatly modified the biological pump and the carbon cycle (Alegret et al., 2012; Lowley et al., 2020). All these factors are believed to play a role in the drops in primary production, carbon export and carbon burial that have been observed in the carbon isotope data from this time (e.g D'Hont et al., 2005; Alegret et al., 2012; Henehan et al., 2019). However, as already said, some benthic groups such as ostracods and benthic foraminifera showed only a minor reduction in biodiversity. This provoked debate on the extent of the biological pumps weakening and pelagic faunal extinction (Alegret et al., 2012). For example, models by Henehan et al. (2019) showed a weakening of carbon export by 50%, which is still enough to sustain the benthic fauna; possibly providing an explanation for its relative stability through the K/Pg (Henehan et al., 2019; Lowley et al., 2020).

In the aftermath of the extinction, a micrite layer

was deposited globally and can be found in localities all over the world, one of these being in the Fiskeler Mb at Stevns Klint (Barlower et al., 2020; Lowley et al., 2020; Störling et al., 2024). The exact source of the global micrite layer is debated but four major factors have been identified: a) Pore water precipitation during diagenesis. b) A backreaction from the vaporization of the limestone target rock during the initial impact caused an influx of CO_2 directly into the ocean. c) an abiotic "whiting event", caused by supersaturation of the $CaCO_3$ in the surface water due to increased alkaline river input and the replacement of eukaryotic primary producers (pelagic calcifiers) by cyanobacteria d) a biologically induced whiting event where the supersaturation is caused by $CaCO_3$ precipitation from bacteria and non-haptophyte algae (Barlower et al., 2020; Alegret et al., 2012). One or a combination of these factors probably caused the mass precipitation and deposition of micrite (Barlower et al., 2020). The exact extent to which these factors contributed is unknown but analysis of the micrite shows a mix of biogenic and abiotic micrite structures (Barlower et al., 2020; Störling et al., 2024).

The Cerithium limestone Mb at Stevns Klint records the earliest marine recovery after K/Pg extinction in a distal location from the initial impact (Schulte et al., 2012). Stable Isotopic data of the global K/Pg extinction recovery particularly in the Cerithium limestone Mb and Fiskeler Mb at Stevns Klint is however surprisingly limited (e.g. Schmitz et al., 1992; Hart et al 2005; Gilleaudeau et al., 2018). The isotopic data that exists mainly $\delta^{13}C$ and $\delta^{18}O$ supports the global trend in isotopic data for the K/Pg except for 5 cm of the Fiskeler Mb at Kulstirenden (Alegret et al., 2012; Gilleaudeau et al., 2018). The Rødvig Fm records a negative trend with a fast recovery right after the extinction (Alegret et al., 2012; Gilleaudeau et al., 2018). That falls in line with recent global paleoproductivity trend where recovery of planktonic primary producers had already started within the Pα zone that has an estimated age of 30 – 200 Kyr (Wade et al., 2011; Lowery et al., 2018). The abrupt negative trend is recorded in the red layer of the Fiskeler Mb at Kulstirenden (Hart et al., 2005). However, the $\delta^{13}C$ isotope trend changes in the Rødvig Formation are of a lesser magnitude compared to other regions globally with value changes around 1 ‰ in $\delta^{13}C$ (Hart et al., 2005; Gilleaudeau et al., 2018). The global value changes in $\delta^{13}C$ differ geographically but range from -1.0-3.0 ‰ and can show value changes around 2-3‰ (Alegret et al., 2012).

3. Method

In this chapter, I will outline my methodology from initial sampling to thin section preparation and final petrographic and SEM analysis.

3.1 Sampling

For this study samples were taken from two different localities, the first sampling site is near Rødvig (55,2540319N Lon 12,3962369E) and the second sampling site is at Kulstirenden near Præsteskov (55,3221226N 12,4506291E). In total 16 samples were taken, 10 from site Rødvig and six from Kulstirenden. The studied sections were divided into subunits A, B, C and D representing observed transition through the Cerithium limestone Mb (Fig. 7). Subunit A represents the transition from a Fiskeler Mb clay stone - marly limestone. Subunit B consists of the main body of the Cerithium limestone Mb until the marker bed of silicified *Thalassinoides* burrows. Subunit B start is marked by the transition from the marly limestone to regular mud/wackestone. Samples around the silicified burrows are part of Subunit C. The D subunit starts from above the marker bed of *Thalassinoides* burrows and lasts until the end of the Cerithium limestone Mb. Sample from Rødvig only show numbers and no letters while samples from Kulstirenden have letters, by example K2 for Kulstirenden and sample 2 for Rødvig. One exception to this labelling rule is the labelling of subunit D as its unique to Kulstirenden (Table 1). Both study sites at Stevns Klint are UNESCO protected. Sampling permission was requested and granted from the Faxe Geomuseum in Denmark.

3.2 Thin sections preparation

From the 16 samples, 28 thin sections were made for petrographic analysis. The samples were cut in halves using a Struers discoplan-TS saw. Selected slabs were cut into rectangles 28x48 mm in size in order to fit the glass slides used for the thin sections. The slabs were then further grinded using a 600 µm grit diamond plate with the Struers RotoPol-25. Once the surface was levelled, the slabs were glued to 28x48 mm glass slides using biocomponent epoxy resin. Both the slabs and glass planes were cleaned with 96% ethanol before gluing. The component proportions between hardener and epoxy were 5:1 Araldite DBF by ABIC Kemi and REN 956 by Huntsman. After gluing, the slabs were left one night in an air oven at 45 °C. Further, the slabs were cut to 1 mm thick with a high precision Struers discipline TS cutting and grinding machine. The slabs were then ground with a 600 µm grit diamond plate and later fined tuned using a 1200 µm grit plate to approximately 30-50 um. Due to the brittleness of the source rock, not all samples could be ground to the same thickness. Samples with poor cementation were dry grounded by hand using 800-1200 µm grit sandpaper to prevent degradation of the sample. To check for variation within specific rock samples and get a higher vertical resolution multiple thin sections were taken from a single rock sample. The thin sections were marked with sample number and a letter showing the position of the thin section within the corresponding rock slab (Table 1).

3.3 Thin section description with optical petrographic microscope

The thin sections were described using a Olympus BX52 microscope at the Department of Geology, Lund University. Pictures were taken using a mounted camera on the microscope (XCam1080PHA). The sample overall petrography and microfacies divisions were described using Dunham's classification (Dunham, 1962) as revised by Embry & Klovan (1971) and Wright (1992). Further subdivision of wackestone was used, bioclastic poor wackestone (10-25% bioclast

content), bioclastic rich wackestone (25-50%). The level of sorting and fragmentation were also described. The level of sorting was described using the sorting classification described in Flugel (2004) as a reference from poor to well sorted. In the scope of figuration, the sorting descriptions were converted to a grading scale from 1-3 where 1 = poorly sorted, 2 = moderately sorted and 3 = highly sorted. Fragmentation was described using the following description parameters. Slightly fragmented (1): When there is some fragmentation of the omnipresent ostracods and bivalves but still a fair number of whole fragments of foraminifera, bryozoans or echinoderms. Moderate fragmentation (2): The amount is in between slightly and highly fragmented. Highly fragmented (3): Most if not all bioclast have some degree of fragmentation. Both fragmentation and sorting were converted into numbers between 1-3 for use in trend curves (Figs. 7 and 9).

Table 1: The Table contains the description for the sample codes used for the sampling and thin sections.

First position = sampling locality.	Second position = vertical position.	Third line = inter-sample position.
Sample starting with letters are from Kulstirenden (Kulstirenden).	Number 1-9 samples in acceding stratigraphical order start of Ce limestone Mb- Korsnæb Mb.	A lower, no letter middle, B above middle, C topmost part of sample.
No letter = Rødvig (Rødvig).	Exceptions: sample 10 is the Maastrichtian (Højerup Mb) reference sample.	Horizontal variation R= right M= middle L = left.

3.4 Point counting

Thin sections were counted on a microscope at the Department of Geology, Lund University using an Olympus Bx50 petrographic microscope equipped with a digital camera (Olympus sc50). An electronic steeping stage was mounted to the microscope's disc stages. The thin sections were counted using Petrog 5. A random grid of points was selected; the number of counts per thin section was set to 250 as the border for statistical significance is at 200 counts (cf. Galehouse, 1971). For the count the bioclasts were classified on order level; Foraminifera's were distinguished between benthic or pelagic. Bioclasts were only counted if the shells were hit by the origo of the crosshair, except for whole ostracods or bivalves' shells. If the crosshair hit inside a complete shell they were also counted as bioclasts. Differences in matrix coloration were divided into three groups: dark, intermediate and light matrix.

3.5 Scanning electron microscopy (SEM)

The samples were analyzed at the Department of geology, Lund University using a variable pressure Tescan Mira3 High-Resolution Schottky FE-SEM equipped with an Oxford EDS detector, at 2 or 15 Kv depending on working distance. Overview and high-detail pictures of the micrite matrix and potential microfacies boundaries were taken. The overview was taken on a scale between 1-5 mm. The high detail pictures were taken at a 100 µm scale.

4. Results

In this chapter, I will present my petrographic descriptions and point counting results starting with Tables for each sample and compiling all my data and descriptions (Table 2 for Rødvig and 3 for Kulstirenden). The point counting data as well as level of sorting and degree of fragmentation for each sample is visualised by a detail log of each site (Figs. 7 and 9) followed by a short description of each subunit and SEM results. This chapter will conclude with a short summary of the results.

4.1 Lithographic description

4.2 Results for Rødvig

This chapter will outline my petrographic descriptions, sample site observations and point counting results for the Rødvig section (Fig.7)

4.2.1 Point counting

The results of the point counting at Rødvig is plotted next to the log in Figure 7. According to the point counting results (Table 2), the lowermost part of the Cerithium limestone Mb is a bioclastic rich packstone dominated by bryozoans and echinoderms (Fig. 8 A). Above sample 3 is a sharp decrease in bioclasts content (sample 3: 26.8%, sample 3b 7.8% bioclasts). In the bottom to middle part of the Cerithium limestone Mb, samples 3b-5 are mainly foraminifera-dominated mudstone (Fig. 8 B, D and G) varying between 5-9% in the total amount of bioclasts. In the upper middle part of the Cerithium limestone Mb, samples 5b-6 are categorized as bioclastic-poor mud-wackestone facies (Fig. 8 C). Towards the upper part of the Cerithium limestone Mb, samples 7-8 show a slight increase in bioclasts, mainly sponges spicules and some bryozoans but it remains a bioclastic-poor wackestone. Both reference samples 9c (Korsnæb Mb) and 10 (Højerup Mb) are bioclastic rich wackestone, dominated by bryozoans.

Table 2. This table compiles my petrographic description of the thin sections made for Rødvig. The data for the point counting is also included in counted samples. The abundance of bioclast is shown in descending order where the first bioclast type is the most dominant.

Thin sections	Dunham microfacies (bioclast content in %)	Short description	Bioclasts	Remarks
2A	Carbonate poor claystone/Bryozoan packstone (50%)	Transitions from carbonate poor claystone/marly limestone to a bioclastic rich wackestone-packstone. Poorly sorted bioclasts. Dominated by larger bioclasts slightly-moderately fragmented. Fragmentation mainly among foraminifera, bryozoans and bivalves.	Larger bryozoans, echinoderms, crinoids and few corals. Smaller bioclasts include: Foraminifera, sponge spicules, bivalves and ostracods.	Most fossils well preserved Partly silicified nodule. Incomplete not fully recovered (NFR) thin section
2B	Bryozoan -packstone	Bioclastic rich wackestone with varying amounts of bioclasts locally borderline packstone. Microfacies boundaries are gradual, Moderate-poorly sorted slightly fragmented.	Bryozoans, echinoderm spines, ostracods, gastropods, bivalves.	Clay seems. Bryozoans reduced in size and less fragmented compared to 2A. NFR
3	Bioclastic rich bryozoan wackestone (26.8%)	Contains a large pocket of Poorly sorted bioclastic rich wackestone, moderately fragmented bioclast. Larger bioclasts in the pocket are sounded by a dark brown matrix. The dark matrix is cut by a sharp bioturbation border. The bioturbated section is a foraminifera dominated bioclastic poor wackestone/mudstone with bioclast decreasing gradually towards the edges of the thin section.	Bryozoans, echinoderms spines, Foraminifera (pelagic and benthic), and some crinoids. Smaller size fractions dominated by ostracods, bivalves and sponge spicules	More fragmented than the previous thin sections. Has a unique fauna due to the addition of a pocket of rework material with large bryozoans, and echinoderm spines associated with some crinoids. The pocket is like the reworked material from Maastrichtian and subunit A. The border looks like a bioturbation a trace with facies similar to samples 3b and 4
3B	Mudstone (7.8%)	Mudstone with locally varying amounts of bioclast, no sharp microfacies borders. Well-sorted, dominated by smaller size fragmented bioclasts. Moderately fragmented	Dominated by calcispheres, echinoderm spines, pelagic foraminifera, ostracods and bivalve fragments, bryozoans	Few single unfragmented bryozoans
4	Foraminiferal Mudstone (5.6%)	Mudstone, well-sorted finer-grained, skeletal fragments dominated by pelagic foraminifera fragments and calcispheres. Few larger bioclasts present, lot of sponge spicules. Slightly- Moderately fragmented.	Pelagic foraminifera some benthic ones, calcispheres, sponge spicules, bivalves and ostracod fragments, bryozoan (rare)	Bioclasts have dark cement like infill.
4b	Mudstone (8.4%)	Mudstone, locally transitioning into a wackestone with bioturbated areas with both sharp and gradual boundaries. Well-sorted, similar sized fragments in both microfacies. Slightly fragmented bioclasts.	Foraminifera, calcispheres, echinoderms, a few small bryozoans, ostracods and bivalve fragments.	Bioclasts in areas of darker matrix share orientation. A second 4b thin-section is closer to wackestone.

5	Mudstone (8.8%)	Mudstone, locally wackestone with bioturbated areas. Gradual microfacies boundaries. The mudstone is more well sorted. The wackestone portion is poorly sorted. Slightly-moderate fragmented bioclasts.	Sponge spicules, pelagic foraminifera, calcispheres, ostracods, bivalve, echinoderm spines, and bryozoans.	Large echinoderm fragment.
5b	Bioclastic poor wackestone (11.2%)	Wackestone with varying amounts of bioclasts, locally bioclastic rich wackestone. A bioturbation trace runs throughout and acts as a microfacies boundary with a gradual but locally sharp transition towards a mudstone. Well-sorted, moderately fragmented.	Ostracods and bivalves, foraminifera pelagic and benthic, calcispheres, echinoderm spines, Sponge spicules, and bryozoans.	Tiny bryozoan fragments.
6	Bioclastic poor wackestone (14%)	Wackestone with patches of more dense areas of bioclastic fragments and bioturbated areas of mudstone. Moderately sorted bioclastic grains are slightly fragmented.	Benthic and pelagic foraminifera, calcispheres, ostracods and bivalve fragments, echinoderms, sponge spicules, gastropods, bryozoan.	Bioclasts in certain areas have similar orientation
7	Mud-wackestone (9.6 %)	Wackestone with varying amounts of skeletal grains and with areas of mudstone with lighter matrix. Gradual boundaries between the microfacies. Well-sorted mostly smaller-sized bioclastic fragments. Slightly fragmented bioclasts	Mainly fragmented foraminifera, calcispheres, ostracods and bivalves fragments, sponge spicules and echinoderms.	
7b	Bioclastic poor Wackestone (11.2%)	Wackestone with varying amounts of skeletal grains and with mudstone areas. Mudstone areas have a lighter matrix. Gradual boundaries between the microfacies. Well-sorted mostly small-sized bioclastic fragments, some intermediate size (around 500μm) in the wackestone. Slightly fragmented	Mainly fragmented foraminifera, calcispheres, ostracods and bivalve fragments, sponge spicules, and echinoderms.	More sponge spicules and calcispheres towards the edge.
7c	Mudstone-wackestone	mudstone with a gradually changing amount of bioclasts. Transitions gradually into a wackestone locally. Well-moderately sorted. Moderately fragmented.	Ostracod and bivalves, sponge spicules, foraminifera and echinoderm spines.	Appears more heterogeneous than 7b. Less foraminifera
8	Bioclastic poor Wackestone (15.6%)	Wackestone going from bioclastic rich to bioclastic poor wackestone. Microfacies boundaries are gradual. Some potential bioturbation traces but the bioclast is unaffected by the traces so might be an epoxy artifact. Moderately sorted with mainly smaller-sized bioclasts, slightly fragmented locally moderate.	Foraminifera dominated, ostracods and bivalves, some calcispheres, echinoderms, a few single bryozoans	Slightly better-preserved bioclasts have less fragmentation compared to the previous samples.

9c (Korsnæb Mb)	Bioclastic rich bryozoan wackestone (36%)	Wackestone with gradually changing amounts of bioclast moderately fragmented and poorly sorted. Dominated by larger-sized bryozoans and some intermediate sized around 500 µm.	Bryozoans, ostracods and bivalve fragments, calcispheres,	Bioclast amount is less than sample 10 but more fragmented.
10 (Sigerslev Mb)	Bioclastic rich bryozoan wackestone (29,6%)	Wackestone, a high amount of larger skeletal fragments at mm scale. In the matrix, few smaller-sized fragments. Homogenous is poorly sorted. Slightly fragmented.	Bryozoans, foraminifera, gastropods, ostracods and bivalves, echinoderms (spines and crinoids), corals.	Less ostracod and bivalve fragments, more calcispheres than in Cerithium limestone. Low fragmentation less than 3 and 2.

Table 3. This Table compiles my petrographic description of the thin sections made from samples from Kulstirenden section. The data for the point counting is also included for the counted samples. The abundance of bioclast is shown in descending order where the first bioclast type is the most dominant.

Thin section	Classification	Short description	Bioclasts	Remarks
K2 (36%)	Bioclastic rich bryozoan wackestone/packstone	Bryozoan wackestone, locally bryozoan packstone, a few small skeletal fragments of ostracods and bivalves. Poorly sorted highly fragmented	Bryozoan, echinoderms (spines, plates and crinoids), ostracods and bivalves, calcispheres.	Incomplete damaged thin sections.
K2b	Bioclastic rich bryozoan wackestone	Wackestone to packstone locally, few small skeletal fragments of ostracods and bivalves. Poorly sorted.	Bryozoan, echinoderms (spines, plates with some crinoids), ostracods and bivalves, calcispheres	Incomplete damaged thin sections. Appears to have slightly more bioclasts then K2.
K3R (10.8 %)	Mudstone-wackestone	Mudstone, locally transitions into a wackestone dominated by sponge spicules, slight bioturbation. Appears well sorted mainly smaller skeletal fragments of foraminifera, moderately fragmented.	Foraminifera fragments, calcispheres, sponge spicules, ostracods and bivalves, echinoderms spines.	reminiscent of sample 7.
K3A	Bioclastic rich wackestone	Bioclastic rich Wackestone well sorted. Dominated by sponge spicules and foraminifera fragments. Moderately-highly fragmented. A fair amount of bioturbation traces.	Sponge spicules, foraminifera, bivalves and ostracods, single bryozoan.	The thin section was cut from a different angle so it gives a different viewing perspective on sample K3 then other K3 thin sections.
K3L	Mudstone-wackestone	Mudstone locally transitions into a wackestone mainly gradual sometimes sharp transitions. Dominated by sponge spicules. Contains nodules partly silicified. Appears well sorted mainly in smaller fragments. Slightly fragmented.	Foraminifera fragments, calcispheres, sponge spicules, ostracods and bivalves, echinoderms spines,	
K3C	Mudstone-wackestone	Mudstone that locally gradually transitions into a wackestone dominated by sponge spicules. Contains nodules partly silicified. Appears well sorted mainly in smaller fragments. Slightly fragmented.	Foraminifera fragments, calcispheres, sponge spicules, ostracods and bivalves, and echinoderm spines.	Mainly mudstone

D1	Mudstone-wackestone (8%)	Mudstone that locally gradually transitions from a lighter mudstone to a bioclastic poor wackestone with a dark matrix. Bioturbated. Well-sorted bioclasts are mainly slightly fragmented.	Echinoderm (mainly spines, one or two crinoids), foraminifera, calcispheres, ostracods and bivalve fragments	Glauconite, unknown fossils which look like large calcispheres
D2	Bioclastic poor wackestone (14%)	Wackestone with varying amounts of bioclastic locally mudstone. Traces of bioclastic rich wackestone. Poorly sorted with high fragmentation. Few small bryozoan fragments. Moderately fragmented Wackestone. However, the mudstone parts are slightly fragmented. A small amount of bioturbation	Both benthic and pelagic foraminifera, calcispheres, echinoderms (crinoids), ostracods and bivalves, and a few bryozoans	Glauconite
D3	Bioclastic poor wackestone (10,8-13,6%)	Wackestone with local mudstone microfacies with gradual and sharp microfacies boundaries. The wackestone facies have varying amounts of bioclasts. Well-sorted slightly fragmented. unclear bioturbations .	Sponge spicules, calcispheres, ostracods and bivalve shells, and foraminifera fragments.	The two D3 thin sections from the same sample slab had slightly different point counting values with 2,8% difference.

4.2.2 Level of sorting and degree of fragmentation

The thin sections described from Rødvig in Table 2 and Figure 7 show that samples 2A-3 constitute poorly sorted microfacies with a varying degree of fragmentation from slightly to highly fragmented. The framework grains in mudstone samples 3b-5b are well sorted with regard to size, but show varying degree of fragmentations. Sample 3b is moderately fragmented and after there is a gradual decrease in fragmentation up section until sample 4b. Successively, the degree of fragmentation increases towards moderate until sample 5b. The middle-upper portion of the Cerithium limestone Mb is varying in both fragmentation and sorting. Sample 6 is moderately sorted grains with a low degree of fragmentation. Samples 7-7b show similar characteristics as both samples are well sorted and slightly fragmented. The top of the Cerithium limestone Mb at sample 8 shows a higher degree of fragmentation and is poorly sorted. Sample 8 is similar in fragmentation and sorting to sample 9 with both samples having a high degree of fragmentation. However, sample 8 is more well sorted than sample 9. In contrast, the Maastrichtian reference sample, sample 10, shows both low degree of sorting and fragmentation.

4.2.3 Lithostratigraphy, subunits and petrography

Rødvig subunit A

Subunit A includes the lowermost part of the Cerithium limestone Mb. Subunit A is a transition layer from the top of the Fiskeler Mb to the Cerithium limestone Mb and it varies in thickness but is commonly around 3-4 cm thick. It shows a transition from a claystone through marly limestone to limestone. Subunit A is represented by samples 2A and 2B. The subunit shows a bryozoan and echinoderm-dominated bioclastic rich wackestone/packstone. Sample 2A contains parts of the Fiskeler Mb claystone, 2b is part of the transition from marly limestone to the proper Cerithium limestone. Only the top limestone part was visible after preparation due to high clay content making the section difficult to prepare. Unlike the rest of the Cerithium limestone Mb subunit A does not show any clear bioturbation.

Rødvig subunit B

Subunit B is a 35- 48 cm thick unit of pale-yellow limestone with bioturbation preserved as brown traces throughout the unit. Subunit B is here represented by samples 3 to 6. The samples show a change from a foraminifera-dominated mudstone with a light matrix to a foraminifera-dominated wackestone with an upwards increasing amount of sponge spicules. The thin section covering the start of the subunit shows a bioclastic rich wackestone (>25% bioclastic content) surrounded by a bioturbation trace of mud-wackestone facies. The larger bioclasts are mainly echinoderm plates, crinoids and bryozoans, they are clumped together within a dark brown matrix. In some parts of the thin section, the matrix shows a light yellowish coloration, corresponding to less well-cemented zones, probably due to bioturbation. Within the bioturbated areas bioclasts density lessens and contains more foraminifera fragments and sponge spicules. The thin-section shows that the Cerithium limestone Mb evolve upwards into a mudstone with gradually fewer bryozoans and dominated by planktonic foraminifera. The foraminifera are often highly fragmented with some more complete specimens visible (Fig. 8 G). Some foraminifers show evidence of dissolution and slight micritisation of the shells. Through the subunit there are clearly visible bioturbation, with traces visible in samples 5b and 3b. Bioturbation is mainly visible as lighter-coloured pathways going through the matrix in a random pattern. The bioturbation sometimes causes sharp boundaries between separate microfacies. The traces in samples 5b, 3b and 3 have different microfacies inside their traces compared to the unbioturbated

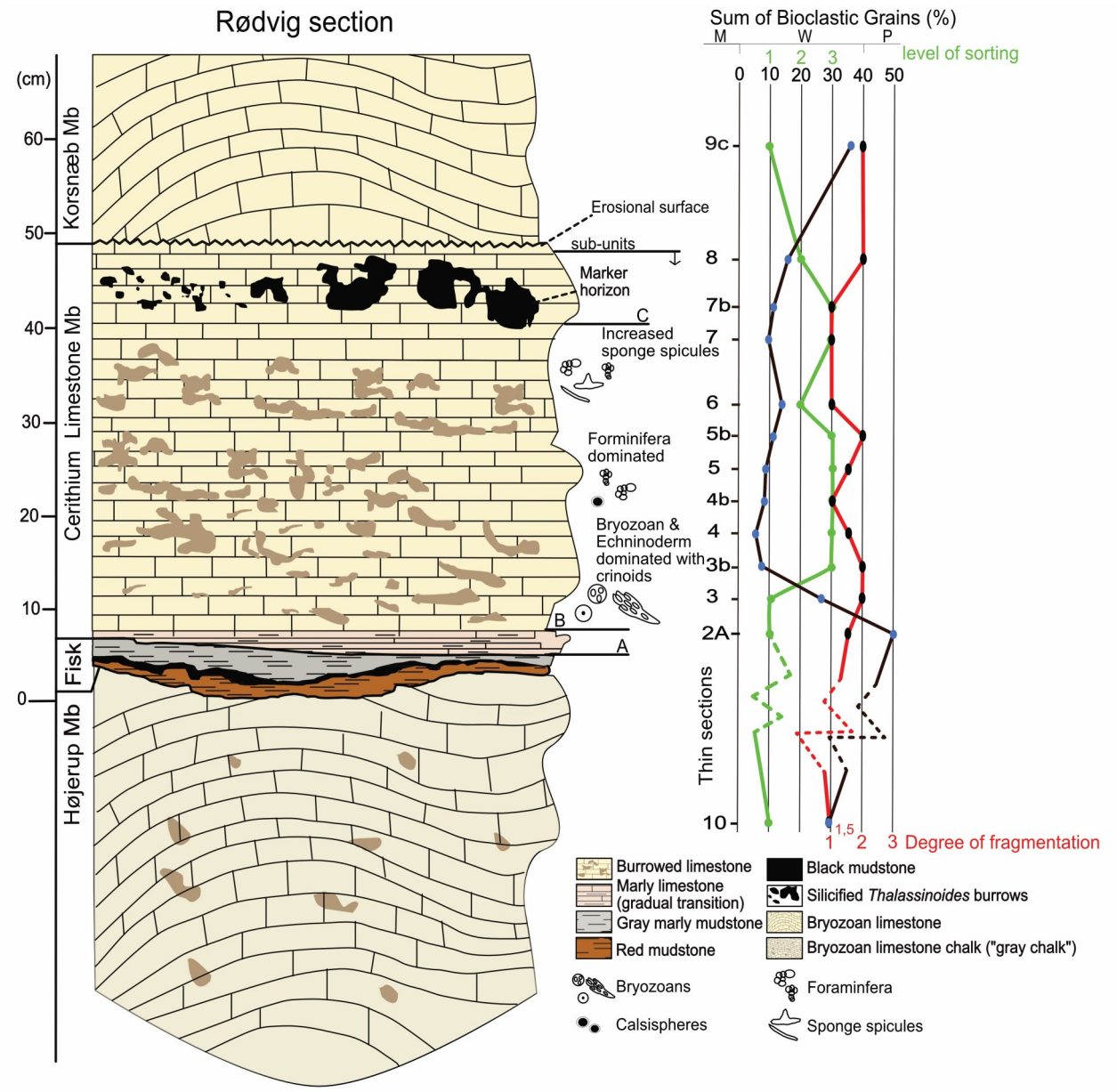

Fig. 7. Detail log of the Rødvig section showing the different members on the left. Fiskeler Mb is abbreviated Fisk. Point counting data and thin section petrographic descriptions from Table 2 are shown to the right of the log with the sample positions matched with the log's vertical scale. The point counting results are plotted with bioclastic amounts (black), estimated degree of fragmentation (red line) and level of sorting (green line). The percentage of bioclastic amounts is grouped by Dunham's classification with mudstone (M) wackestone (W) and packstone (P), respectively. The exact height of sample 10 within Højerup Mb is not known (shown as dashed lines) although it is within the uppermost meters of the Højerup Member. The degree of fragmentation is classified on a scale between 1-3 (only reached 2 in the Rødvig samples): 1 = slightly, 1,5 = slightly/moderate, 2 = moderate, 3 = high. The level of sorting is classified 1-3: 1 = poor 1,5 = poor-moderate 2 = moderate 3 = well. The subdivision

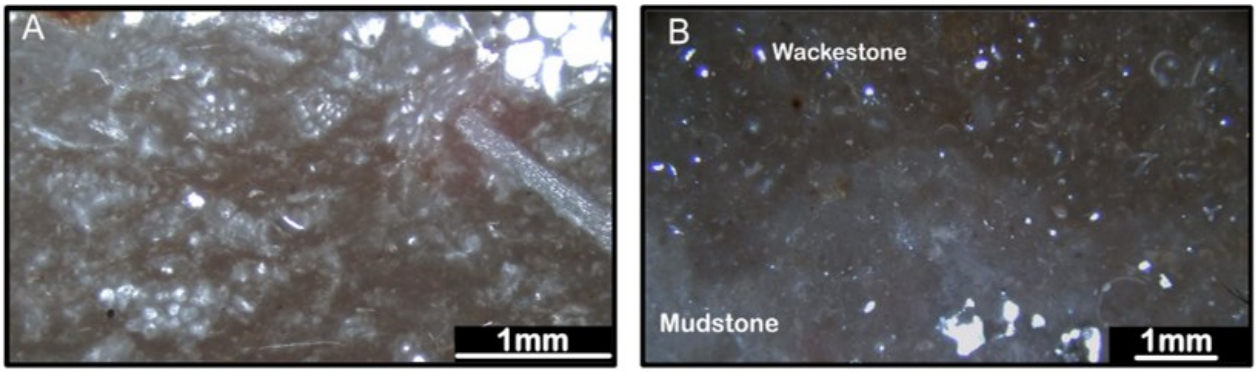

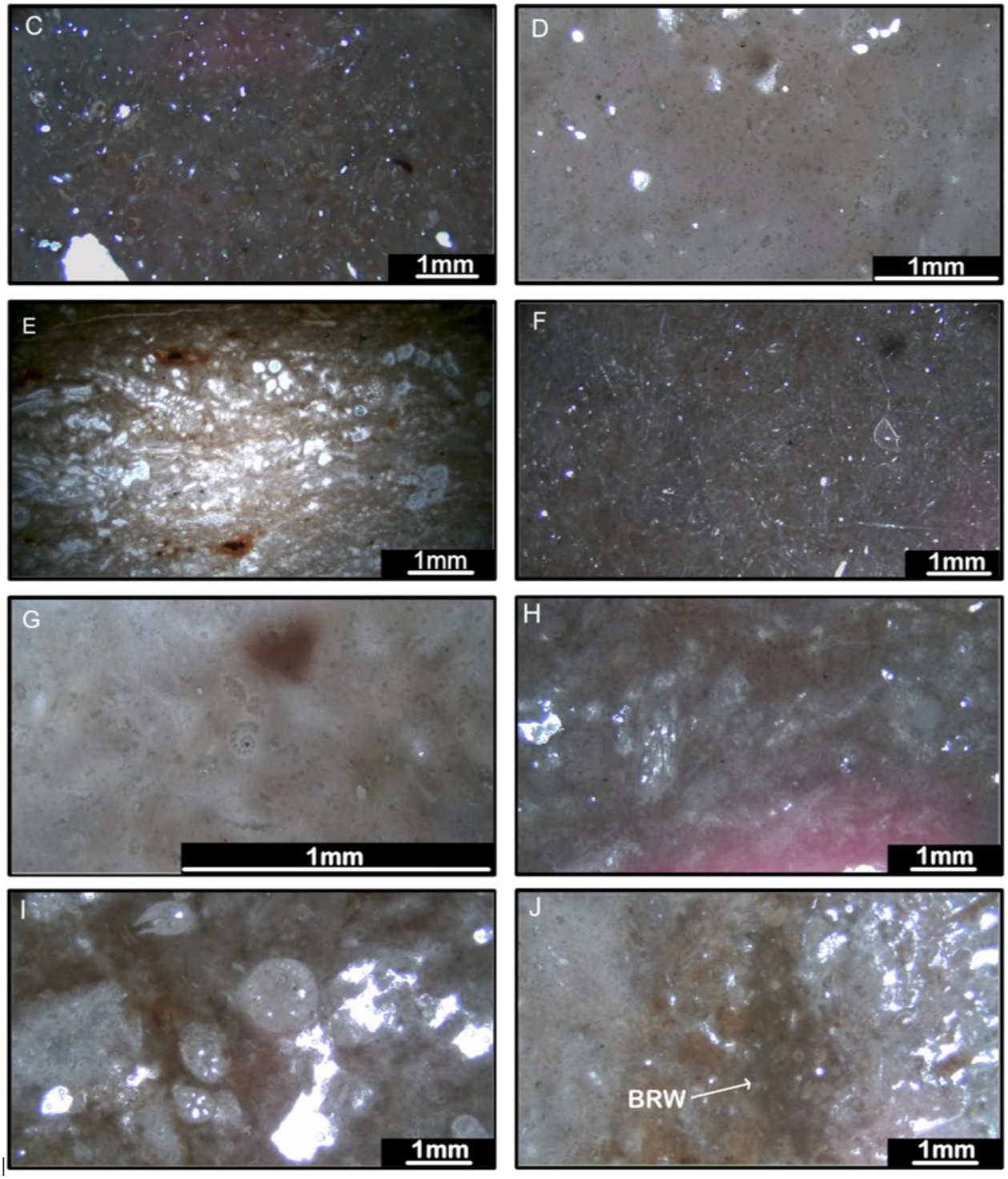

Fig. 8: Microphotographs taken with an optical microscope of selected thin sections showing different microfacies and other important structures. Description for each picture is as follows: A = Sample 2A, showing an example of the bioclastic packstone microfacies at Rødvig, B = Sample 5B, showing a gradual transition from wackestone to mudstone, C = Sample 5b, showing an example of the bioclastic-poor wackestone microfacies 5b, D = Sample 4, showing an example of the foraminifera-dominated mudstone microfacies, E = Sample K2 from Kulstirenden locality, showing the bryozoan packstone microfacies, F = Sample K3A, showing a well sorted, bioclastic rich wackestone, dominated by sponge spicules and foraminifera fragments. G = Sample 4b, showing well preserved foraminifera in mudstone, H = Reference sample from the Korsnæb Mb, 9C, showing a bryozoan wackestone, I = Maastrichtian reference sample, 10, showing a bryozoan wackestone, J = Sample D2, showing small pocket of highly bioclastic rich wackestone (BRW) that shares similarities with the wackestone in samples 3 and K2.

parts. The micrite matrix in this section contains gradually changing amounts of bioclast as well as several 20-50 µm rounded to subrounded dark particles, interpreted as griding artifacts. Samples 4, 4b and 5 contain mainly foraminifera-dominated mudstone facies but locally transition into a wackestone, mainly gradually but sometimes sharp. Towards the top of the subunit there is an increase in sponge spicules that continues into subunit C but foraminifera are still dominating except in sample 5b where ostracods and bivalves become more prevalent.

Rødvig subunit C

Subunit C is a 25-35 cm thick unit that includes the marker horizon of *Thalassinoid*es burrows and above (samples 7-8). This upper part contains mainly a bioclastic-poor wackestone dominated mainly by foraminifera fragments, but in some places a larger amount of bivalve and ostracod fragments, or a notably higher amount of sponge spicules. The bioclastic content shows a small increase towards the top of the unit. The degree of bioturbation is unclear as there are no distinct burrows, except the large *Thalassinoid*es, in these samples. This subunit also contains partly silicified flint nodules. The microfacies in these samples vary between mud- and wackestone with gradual microfacies boundaries.

4.3 Result for Kulstirenden

In this chapter will outline the petrographic descriptions and point counting results for the Kulstirenden section (Fig. 9).

4.3.1 Point counting results

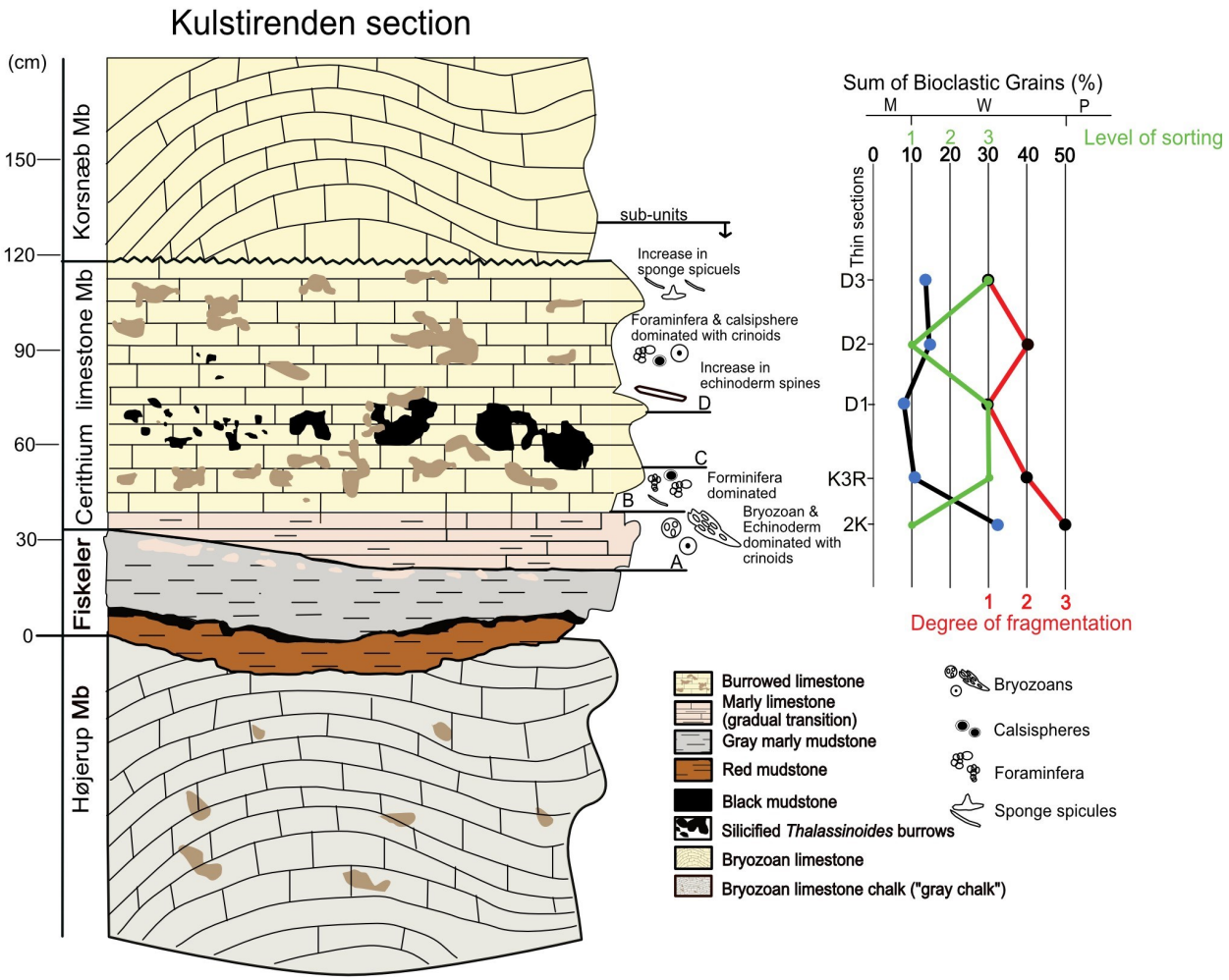

Fig. 9: Detail log of the Kulstirenden section showing the different members on the left, Fiskeler stands for Fiskeler Mb. Point counting data and thin-section petrographic descriptions from Table 3 are shown to the right of the log with the samples matched with the log's vertical scale. The point counting results are plotted with bioclastic amounts (black), estimated degree of fragmentation (red line) and level of sorting (green line). The percentage bioclastic amounts are grouped by Dunham's classification with mudstone (M) wackestone (W) and packstone (P) respectively. The degree of fragmentation is classified between on a scale 1-3: 1 = slightly, 1,5 = slightly moderate, 2 = moderate, 3 = high. Level of sorting is classified 1-3: 1 = poor 1,5 poor-moderate 2 = moderate 3 = well. The subunit divisions of the Cerithium limestone Mb A-C are shown to the right of the log. The 0 in the section is the base of the Fiskeler Mb located approximately 4 m above sea level. The thickness of the Højerup Mb at the locality is not measured. Highlights of the general fossil content from the samples are shown next to the log.

The point counting results for the Kulstirenden section are shown in Table 3 and are plotted in Figure 9. The lower part of the Cerithium limestone Mb is represented by samples K2 and K2b. The bioclastic content of sample K2 is 36% and therefore classified as bioclastic rich wackestone, dominated by bryozoans and echinoderm. Sample K3R included 10.8% bioclasts and was classified as a bioclastic-poor wackestone. The upper part of the member starts as a mudstone with 8% bioclasts. The rest of subunit D shows a consistent bioclastic poor wackestone with a bioclast amount ranging from 10,8-15%.

4.3.2 Level of sorting and degree of fragmentation

The thin sections described in Table 3 and Figure 9 from Kulstirenden show that samples K2 and K2b are poorly sorted and highly fragmented. Sample K3-D1 in the lower and middle part of the Cerithium limestone Mb are well sorted but with a varying degree of fragmentation. The green and red lines intersect at D1 showing a well sorted and slightly fragmented sample. Going from D1 to D2 the sorting and fragmentation trends sharply change to a poorly sorted and highly fragmented wackestone, and then returning to a well sorted and slightly fragmented wackestone at D3 (Fig. 9).

4.3.3 Lithostratigraphy, subunits and petrography

Kulstirenden subunit A

Subunit A at Kulstirenden (samples K2 and K2b) includes the transition layer from marly limestone in the uppermost Fiskeler Mb (in sample K2) to the carbonate-rich, lower part of the Cerithium limestone Mb (Fig. 9). The marly limestone of subunit A varies in thickness but is approximately 5-10 cm thick. Sample K2 is a bryozoan bioclastic rich wackestone with crinoids and echinoderm spines.

Kulstirenden subunit B

Subunit B at Kulstirenden is less thick as compared to subunit B at Rødvig and is represented by a single sample (K3) from which four thin sections were made (K3R, K3L, K3A and K3C). The sample shows a mud-wackestone where the mudstone portions are dominated by foraminifera and calcispheres, whereas the wackestone portions are dominated by sponge spicules. K3A however has been produce parallel to the stratigraphy, whereas all the other were produce perpendicular. It has bioturbation traces unlike the other K3 thins section and it also has a large amount of sponge spicules throughout the thin section.

Kulstirenden subunit C

A clear subunit C could not be defined at Kulstirenden.

Kulstirenden subunit D

Subunit D is above the marker horizon of silicified *Thalassinoides* burrows at Kulstirenden and is approximately 50 cm thick. The subunit is represented by three samples (D1-D3). The lower D subunit is a mudstone dominated by echinoderms and with a light matrix that locally transition into darker wackestone microfacies. The middle part of subunit D contains a bioclastic-poor wackestone, dominated by both pelagic and benthic foraminifera and echinoderm spines and crinoids. In D2, there is a small pocket of bioclastic rich wackestone which shares similarities to the bioclastic rich wackestone in sample K2 and sample 3 at Rødvig. However, the bioclasts are highly fragmented making identification hard. The D subunit shows bioturbation traces in D1 and D2 that have clear differences in bioclastic amount within the traces. In Sample D3 bioturbation amount is unclear. The top of subunit D (sample D3) is a bioclastic-poor wackestone with varying amounts of bioclasts, which are dominated by sponge spicules.

4.4 SEM Analysis

SEM analysis was done on four thin sections (samples 3, 3b, 4 and 7). Sample 3 showed a micrite with locally slight cementation. The transition from dark to light matrix is not possible to see on the SEM picture. Both micrite in samples 3 and 3b (Fig. 10 3A1-A2 and 3b A and 3b B) show the same grain size and composition. Samples 4 and 7 show a micrite with slight cementation, however much of the matrix is not visible due to the smearing of the surface during the grinding (Fig. 11 A1, A2 and B). There does not seem to be a discernible variation between the dark and light micrite in sample 4 (Fig. 11 A1 and A2). Contaminations were common through the thin sections like the ones seen in Figure 11 A2. Most common was the smearing effect and fragments of bioclasts being ripped up during the grinding.

4.5 Descriptions summary

The Cerithium limestone Mb at Stevns Klint is a pale yellowish limestone with brown bioturbation tracks scattered throughout the section. A prominent flint band of *Thalassinoides* burrows is noted at both localities and is most likely an important marker horizon (see also Hart et al 2005). As it occurs in different position relative the upper boundary of the unit in the two studied localities, it helps to interpret the preservation and stratigraphic completeness of the two sections, the Kulstirenden being the longer lasting. At Rødvig, the Cerithium limestone Mb ends at the top of the *Thalassinoides* marker horizon, while in Kulstirenden, the limestone continues above that horizon as subunit D. The Cerithium limestone Mb is a heterogenous, micritic bioturbated limestone with varying content of bioclasts (Tables 2 and 3; Figs. 7 and 9). Most bioclasts are fragmented, mainly the smaller bioclasts like ostracods, foraminifera and bivalves (Fig. 8). The limestone appears generally porous with most pores and cracks containing varying amounts of recrystallized microsparite. The Cerithium limestone Mb is generally poorly cemented but has varying degrees of silicification through the unit making it more compact. The silicification mainly increases up-section

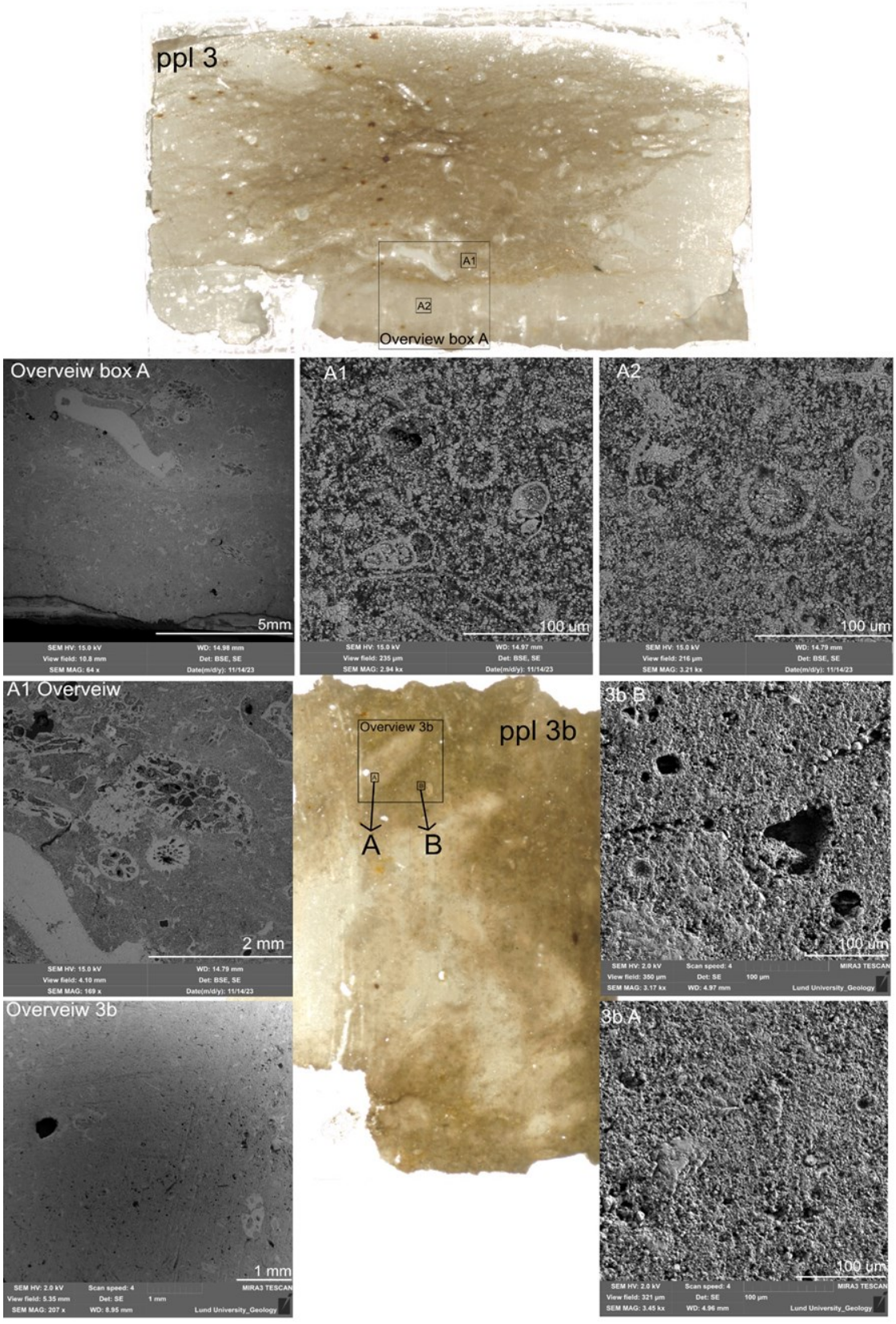

Fig. 10: SEM pictures from thin sections 3 (ppl 3) and 3b (ppl 3b) showing differences in the matrix surface at different scales. The position and size of the SEM pictures are shown by the boxes on the plain polarized light (PPL). picture of each thin section.

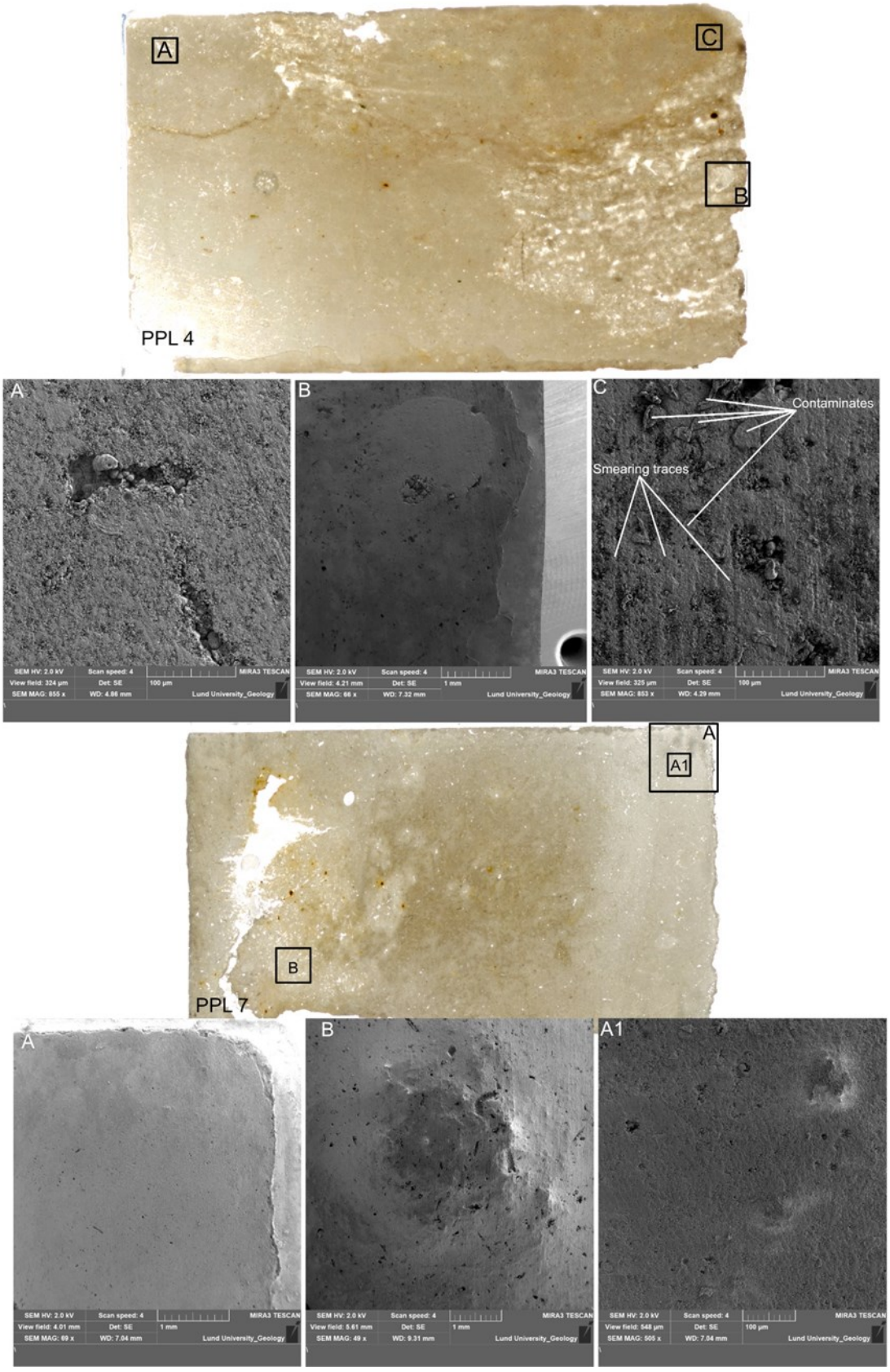

Fig. 11: SEM pictures from thin sections 4 (PPL 4) and 7 (PPL 7) show differences in the matrix surface at different scales. Pictures of the thin sections are shown plain polarized light (PPL) with boxes on each picture marks the SEM pictures positions within the thin section. SEM pictures are shown below its corresponding thin section.

with silicification being highest in and around the marker horizon with silicified *Thalassinoides* burrows. The limestone contains three different microfacies: a mudstone, a bioclastic-poor wackestone (10-25% bioclasts) and a bioclastic rich wackestone (25-50% bioclasts). Both sites show that the Cerithium limestone Mb starts with a bryozoan /packstone with crinoids. The limestone starts approximately with a 5 cm-thick bioclast-rich wackestone to packstone but rapidly transitions to a mudstone with around 7-8% bioclasts. In the mid-section of subunit B the Cerithium limestone Mb transitions into a bioclastic-poor wackestone. The bioclastic-poor wackestone continues throughout the next subunit and until the top of the unit in the Rødvig section. Bioturbation exists through subunit B but is however not visible in subunits A. Fragmentation and sorting vary through the Cerithium limestone Mb and show no consistent patterns as the trend lines overlap at some samples (Fig. 7) where highly sorted samples are low in fragmentation, but in many samples it differs. The Kulstirenden locality (Table 3 and Fig. 9) shows a reduced B-C subunit as compared to at Rødvig (Table 2 and Fig. 7). Subunit A-B at Kulstirenden shows a transition from a poorly sorted, highly fragmented bioclastic rich wackestone, to a well sorted slightly fragmented bioclastic-poor wackestone. Subunit D has multiple changes in both bioclastic content, fragmentation and sorting. Initially, there is a slight decrease in bioclastic content from a bioclastic-poor wackestone into a mudstone in the lower part of subunit D. In the mid to top of subunit D the limestone transitions back into a bioclastic-poor wackestone. The D subunit shows a slight indication of changes in faunal composition throughout the subunit mainly being foraminifera dominated with crinoids and singular fragmented bryozoans visible. The sites also show a similar petrography up to the *Thalassinoides* marker horizon, except thickness variations and minor differences in the abundance of certain bioclasts, like sponge spicules and foraminifera.

5. Discussion

5.1 Method errors and biases

Within the point counting there are minimal errors outside the expected bias that comes with bioclast identification. The 250 counts are considered as statistically representative for each sample, as 200 points have been statistically proven to be the cutoff point in the statistical variability for this method (cf. Galehouse, 1971). However, as the whole thin section is counted the microfacies variations within the thin sections are not quantified. The microfacies variations within samples are thus deduced only from observation. This highlights the difficulties to classified certain thin section, strengthens by the slight difference between bioclastic rich mudstone and bioclastic-poor wackestone. Indeed, most thin sections varied within a 5% difference of the cutoff point at 10% bioclast content for the mudstone/wackestone boundary. As mentioned in 3.3 a further subdivision was made to distinguish the wackestone microfacies due to the high variance in wackestone bioclastic content results.

The difficult sample preparation may have increased the source of errors. Due to the soft and poorly cemented nature of the limestone, a smearing effect occurred during polishing, spreading the fine-grained micrite as an even and very fine-grained film over parts of the thin section. This could have destroyed or obscured bioclasts or potential matrix variation. Such smeared areas, which were clearly identified in the SEM, were not visible under a plane polarised light microscope. Furthermore, during the SEM analysis, the smearing was mainly visible on the matrix and only to a limited extent on the bioclasts. Therefore, the smearing had probably little bearing on the point counting result, but it is still an important factor to consider especially for SEM analysis. For future studies the samples could be shortly soaked in light acid to remove some of the excess material before viewing.

For the other metrics that are not quantitatively measured, like fragmentation and level of sorting, there are more biases to consider. In this case, however, predefined classifications have been used, which reduces potential errors. The degree of fragmentation poses more problems as the definitions of what exactly high and low fragmentation is unique to this study is particularly subjective. Terms like high and low are in this study more accurately referred to as higher or lower within this sample set. Thin sections with more abundant and larger bioclasts can appear to be more fragmented as fragmentation becomes easier to discern compared to a mudstone with fewer and smaller fragments. However, during the description of fragmentation this bias was taken into account for the bigger samples as I kept this in mind and would rather under than overestimate these samples.

The level of sorting has a similar bias since size differences in bioclast are easier to see in a wackestone than a mudstone. Therefore, these counts are subjective descriptions and cannot be used to make conclusions by themselves. However, they can indicate areas for further study and potentially strengthen arguments together when combined with other quantitative data. The data is therefore still vital for identifying future study areas for the Cerithium limestone Mb. Given the biases mentioned above, the level of sorting as well as the degree of fragmentation are primarily viewed as indicators of trend changes rather than exact measurement of fragmentation or sorting levels

5.2 Petrography of the Cerithium limestone Mb

At Rødvig, the results show a clear heterogeneous limestone (Table 2, Fig. 7) with the lower part of the Cerithium limestone Mb (samples 2 and 3) consisting of a bryozoan bioclastic rich wackestone/packstone with a faunal assemblage dominated by bryozoans and echinoderm spines associated with crinoids (Figs. 7 and 8). Thin sections 2A and 2B were not fully recovered, it is thus not possible to say if the lower marly limestone layer of subunit A is also a bioclastic rich wackestone/packstone. The microfacies of subunit A are unique and do not reoccur in any other part of the limestone. The absence of strong bioturbation is another typical feature of this unit. In contrast, subunit B of the Cerithium limestone Mb is highly bioturbated, as

best seen in samples 3 and 3b (Fig. 10 ppl 3 and ppl 3b). The start of subunit B (sample 3), however, contains inclusions of bryozoan packstone typical of subunit A, but as this packstone is surrounded by a bioturbation trace of foraminifera-dominated mud/wackestone it is not included as a part of subunit A. The bioturbated parts in subunit B generally show mud/wackestone microfacies like the rest of the limestone. Because of the bryozoan packstones of subunit A unique placement at the beginning of the Cerithium limestone Mb and the fact that this bryozoan packstone is similar to the Maastrichtian sample (sample 10), we consider subunit A as mainly representing the reworking of material from the underlying Maastrichtian Højerup Mb. The upward transition to a foraminifera-dominated mudstone likely represents the continuation of the original deposition conditions of the Cerithium limestone Mb, had it not been interrupted by the introduction of reworked Maastrichtian sediments. The foraminifera in the mudstone of subunit B (samples 5 and 4) varies between being highly fragmented or fully articulated, and there is evidence of dissolution and micritisation of foraminifera shells. A recent study by Störling et al. (2024) suggested that the reason for the many studies finding variation in foraminiferal species leading to different foraminiferal zonations could be due to the high local variation in the degree of preservation of foraminiferal shells. In subunit C (samples 6-7) there is a slight increase in bioclastic content mainly due to an increase in the abundance of calcified sponge spicules. A larger deposition of sponge spicules is likely the cause for the secondary silicification that formed the conspicuous *Thalassinoides* flint band in the upper Cerithium limestone Mb. The silica in the sponge spicules probably dissolved during early digenesis, as the burrows would need to be already stabilised but still have enough porosity for the remobilising silica to be able to reprecipitated in the *Thalassinoides* burrows. A slight increase in bioclasts content is evident in the uppermost part of the Rødvig section, top of subunit C, (sample 8). However, this increase is only 4.4% (Table 2, Fig. 7).

The Kulstirenden section also shows a heterogenous Cerithium limestone Mb starting with subunit A that consists of a bryozoan bioclastic rich wackestone. The K2 thin section was not fully recovered so it is not possible to say if the entire marl layer is a wackestone/packstone. However, as the samples from subunit A at Rødvig (2A, 2B) show the same wackestone/packstone petrography with similar faunal composition it is likely that most of subunit A should be a wackestone/packstone at Kulstirenden as well. As in Rødvig, subunit A is unique to the lowermost portion of the Cerithium limestone. Subunit B at Kulstirenden is thinner as compared to at Rødvig and only one thin section from one sample (3K) was produced. The sample shows a similar petrography to Rødvig with a foraminifera-dominated mud/wackestone, except for having an increased amount in siliceous sponge spicules. The top of subunit B at Rødvig does as well show an increased content of sponge spicules. If the *Thalassinoides* burrows is a reliable marker horizon, subunit B is condensed at Kulstirenden, especially the lower part of this unit. Subunit C could not be clearly defined at Kulstirenden however, the increase in sponge spicules seen in subunit B at Kulstirenden is also a characteristic of subunit C, it could therefore indicate that subunit B at Kulstirenden is a combination of subunit B and C but more sampling is needed to confirm this. Subunit D is unique to Kulstirenden. The D subunit shows a heterogenous composition between mud and wackestone. D2 also shows pockets of more packstone /bioclastic rich wackestone material (Fig. 8 J). This material is likely reworked material due to bioturbation however as it is above the *Thalassinoides* horizon the exact organism responsible is uncertain. As the material does not share many similarities with the Korsnæb Mb reference sample (9c), it is unlikely to be reworked from later Danian time. It shares more similarities with the Højerup Mb reference samples and the bioclastic rich wackestone in samples 2k, 2A and 3. For example there appear to be bryozoan fragments visible that share some similarities with bryozoans found in samples 3 and 2k. However, as this pocket is very small and fragmented, the exact identification is difficult and therefore the material's origin cannot be determined with certainty. The rest of subunit D does have similar bioclasts content compared to subunit B with echinoderms foraminifera and sponge spicule being common. However, it does also contain a few singular bryozoans and crinoids. These differences do indicate that subunit D is a separate unit of the Cerithium limestone Mb, as petrographic facies or faunal composition differ from subunits B and A, but still shares the common heterogenous petrography and bioclasts of the Cerithium limestone Mb as a whole.

5.3 The heterogeneity of the Cerithium limestone

As outlined in section 5.2, the Cerithium limestone Mb in both localities has a heterogeneous composition on the microscale with different matrix-rich carbonate microfacies. The vertical variations within the Cerithium limestone Mb are shown to be minor except for sub-unit A. However further differentiations can be observed within a single thin section sample. In most of the samples the microfacies changes appear to be mainly gradual; a good example can be seen in samples 5b (Fig. 8 B) where there is a clear wackestone to mudstone transition. However, sharp boundaries occur, most commonly at the base of subunit B (samples 3, K3L and 3b). This is most likely due to bioturbation burrowing through the reworked material separating the material and condensing bioclasts in certain areas, creating sharp boundaries. A good example of this is seen in sample 3 (Fig. 10 3 ppl) where there is a sharp boundary between the bioclastic rich and bioclastic-poor wackestone facies.

Facies heterogeneity is often related to changes in sea level or water current velocities. However, the heterogeneities in the Cerithium limestone Mb are unlikely to be due to shifts in energy regime, as evidenced by the gradual and minor vertical variation in bioclast distribution, approximately 8-13% at both sites, indicating a consistently low-energy environment. It is noteworthy that these numbers may be subject to standard statistical variance and can only be applicable to the Rødvig sites, as subunit B is only

represented by one sample at Kulstirenden. The clear microfacies differences visible within the thin sections (Fig. 8 B and J) have a random distribution and would have been more systematic if caused by changes in energy regime. Moreover, the changes are occurring mainly on a microscopic scale making it too small to be an effect of larger changes in energy regime. However, variance in the degree of fragmentation as well as different levels of sorting and slight bioclastic increase throughout both sections could indicate some level of systematic sorting. This would however have to be confirmed with more quantitative analysis of the fragmentation degree and sorting level. The distribution pattern of the different microfacies is most likely an effect of repeated burrowing during and after deposition. A part of the bioturbation seen in the Cerithium limestone Mb could be linked to the *Thalassinoides* burrows. However, the *Thalassinoides* burrowing cannot explain the microscopic gradual changes in microfacies seen within samples. Therefore, bioturbation from smaller micro-sized organisms must have occurred as well. The exact origin of these microscopic burrows cannot be determined with the data in this paper.

5.4 Lateral variations between Rødvig and Kulstirenden

The petrographic descriptions at Rødvig and Kulstirenden show both similar microfacies, ranging from mudstone, bioclastic-poor wackestone, bioclastic rich wackestone and packstone. Differences in faunal composition, bioclastic abundance and the order in which these microfacies occur are observed between the two sites. The A subunit has the same facies and bioclastic content at both Rødvig and Kulstirenden, with thickness being the only difference (Fig 7 and 9). Subunit B is substantially thinner at Kulstirenden than at Rødvig. This could be due to less accommodation space, but more likely variations in the local sea-floor environment. A lack of accommodation space is unlikely as the units at Kulstirenden are overall thicker than at Rødvig. The thickness variation could also be due to the unit not covering the same time frame. However, the *Thalassinoides* are connected to hardgrounds and burrow down at a consistent depth (30 – 50 cm) through multiple members at Stevns Klint (Surlyk et al., 2006). Because of this, it is used as a marker bed at Stevns Klint and therefore it is assumed to be a marker horizon covering a consistent time frame also for the Cerithium limestone Mb. The marker horizon forms a seemingly consistent line that follows the natural mounding for the Cerithium limestone Mb. Therefore, it is unlikely that there is a large time discrepancy between the time of formation of the marker horizon between the sites. With that said, high resolution isotopic analysis of limestone enclosing the marker horizon is needed to settle this question. Instead, the condensation could have been caused by an increase in water currents washing out more of the matrix of subunit B at Kulstirenden. However, then there should be a more bioclastic rich wackestone in sample K3, which is not the case as there is still a large amount of matrix visible in sample K3. The bioclastic content of the B subunit varies between the sites but only in the abundance ratio of different bioclasts. This is mainly due to the increase in recrystallized sponge spicules seen in K3 at Kulstirenden, but not appearing at Rødvig until sample 7. Important to note, that if the bioclastic content of samples 4-7 from Rødvig was combined it would be expected to look similar to what is seen in sample K3 from Kulstirenden. This makes the theory of condensation more likely, however, the exact mechanism for the condensation remains uncertain. Changes in water current speed, if they occurred, should be visible at other parts of Kulstirenden so until more evidence can be gathered for this it is not possible to know the exact mechanism for the condensation of subunit B.

Samples close to the *Thalassinoides* burrows at both sites and subunit C at Rødvig have shown an increase in sponge spicule in the form of recrystallized calcite, most likely a remnant from the silicification of the *Thalassinoides* burrows. The *Thalassinoides* silicification is an effect of post-depositional remobilization of silica, caused by an overabundance of silica due to a large amount of sponge spicules being deposited. There is secondary silica also outside of the *Thalassinoides* burrows with partly silicified flint nodules being found in some samples but mainly in the samples around the marker horizon in Kulstirenden (Table 3). These partly silicified flint nodules were however not seen in the Rødvig localities (Table 2). The sponge spicules, however, are mainly seen towards the edge of thin sections from both sites. This is probably an effect of the edges being grided thinner during preparation. This in turn suggests that sponge spicules could be present to a larger extent through the unit, but that they are less visible in thicker thin sections, indicating a bias in the data. This is further reinforced by sample K3A, which is cut from a different angle on the sample compared to the rest of the K3 samples, and which shows an abundance of sponges spicules. The fact that this increase is present in multiple thin sections at a similar level in both Rødvig and Kulstirenden indicates that this is a change in bioclast composition rather than an effect of the sample preparation.

At Kulstirenden, the Cerithium limestone Mb continues above the *Thalassinoides* marker horizon, whereas it is not preserved above this horizon at Rødvig. This continuation at Kulstirenden is represented by subunit D. This unit shows similar general facies as the underlying Cerithium limestone Mb but show a slight variation in bioclastic composition. This part has probably been eroded away at Rødvig as evidenced by the erosional hardground toping the member at both sites. In Kulstirenden, bioclastic content differs showing a wackestone with abundant crinoids associated with foraminifera and a reoccurrence of bryozoans. This alone is not enough to conclude that the D subunit is a continuation of the Cerithium limestone Mb as all these bioclasts are present throughout the member at both sites. Carbon isotope analysis could help solve this issue by showing if subunit D has a unique isotopic ratio. This could also help to confirm that subunit B at Kulstirenden is a condensed version of subunit B at Rødvig as they should still share a similar isotopic ratio. The temporal origin of these subunits would also help in confirming if the *Thalassinoides* marker horizon covers a similar time at both sites.

5.5 Depositional environment of the Cerithium limestone Mb

Even with the extensive petrographic data presented in this paper, due to the lack of a quantitative species-level analysis of the faunal assemblage, making a concrete assessment of the depositional environment after the K/Pg at Stevns Klint is difficult. However, there are important indicators that can be explored. The fact that the reworked material exists in the same unit on the two different sites indicates that the reworked bryozoan packstone could be a consistent layer throughout Stevns Klint. The exact reasoning for this reworking is hard to explain with this limited data set. However, a likely cause is the high acidification confirmed to have occurred globally through the K/Pg mass extinction (e.g. Alegret et al., 2012; Henehan et al., 2019; Lowley et al., 2020). Even if the acidification was not strong enough to provoke partial dissolution, it would at least inhibit early cementation to occur and in turn destabilizing the Højerup Mb mounds. Moreover, considering the uneven paleo-bathymetry caused by the Højerup Mb mounds, creating relief, it would be natural for material to be transported. The resulting slope caused weak underwater currents to form. This would in turn cause the unconsolidated material deposited on top of the Højerup Mb mounds to collect in the low points of the mounds. Small yet prevalent transport would also explain the level of fragmentation seen in the larger bryozoan clasts in the lower samples 2B, 3 and K2 (Fig. 7 and 9). It is known that currents in the area where WNE-ESE direction facing the position of the crest axis of both the Maastrichtian and Danian mounds. Additionally, underwater valleys facing the same direction have been found in the nearby Kattegat Sea (Surlyk et al., 2006; Lykke-Andersen & Surlyk, 2004). It is therefore probable that the currents were similar during the deposition of the Cerithium limestone Mb. There is no obvious evidence of energy regime changes at any of the studied sites. Because of this the Cerithium limestone Mb was likely deposited in a deep low energy environment below the storm wave base. However, the presence of fragmentation and sorting differences could indicate the presence of weak underwater currents.

The fragmentation may indicate some sort of transport and the smaller isolated rounded bryozoans seen in samples 6 and 5b could indicate transport of material after the deposition of the reworked subunit A. The presence of well-sorted material with different fragmentation could indicate some sort of changes in bioclast size distribution over time. However, since the time resolution of the section is uncertain it is hard to say if these are smaller isolated events of underwater current changes or something more long-term on a larger regional scale. Since the data on the degree of fragmentation (Figs. 7 and 9) does not indicate any clear cyclicity or systematic changes it is unlikely that there were any large changes in the energy regime. If some level of smaller underwater currents did occur, they may have been caused by the gradient differences in the paleo-bathymetry caused by the Maastrichtian Højerup Mb mounds. This difference would cause settling or loosened benthic bioclast to undergo a small amount of transport from the flanks of the mounds to the bottom. However, if this transport is large enough to cause the degree of fragmentation seen in many of the bioclast groups is uncertain. It is also important to note that Surlyk (2006) has attributed strong underwater currents as the cause of the many erosional hardgrounds present in both the Højerup and Korsnæb Mb at Stevns Klint. The Cerithium limestone Mb is topped by an erosional hardground at both sites that likely has a similar origin. If strong currents like this did affect even deeply deposited sediments it keeps the possibility that currents did in fact reach the deeper sediments and could have a contributing effect on the deposition of the Cerithium limestone Mb. However, this would still be a secondary factor as the microfacies changes are random and is therefore more likely to be caused by bioturbation. Therefore, quantitative data on the sorting and fragmentation levels needs to be collected to make any concrete conclusion about the extent of any potential inorganic depositional control factors.

In regard to the faunal assemblages within both localities, we see mainly foraminifera, echinoderm spines, bivalves and ostracods, with some levels showing an increase in bryozoans due to the Maastrichtian reworking, or sponge spicules possibly due to the sample preparation method. The foraminifera is represented by both benthic and pelagic forms in the reworked bryozoan-dominated parts. Therefore, I believe that the most representative samples for the faunal composition in the earliest Danian of the Cerithium limestone Mb is the middle to upper samples of the B subunit (samples 5-7); the foraminiferal mudstone that transition into wackestone with increased sponge spicules. Bryozoans are still present but to a smaller extent with the dominating bioclast changing between foraminifera, echinoderm spines, ostracods and bivalves and sponge spicules. One exception is the D subunit as Kulstirenden which does seem to show a unique faunal composition compared to the other units at both sites. The data presented in this thesis does however indicate that the faunal composition is heterogeneous like the petrography and is more dependent on post-depositional reworking due to bioturbation rather than being an effect of *in situ* faunal changes, apart from subunit D at Kulstirenden. However, a more quantitative analysis of the faunal composition is needed in order to know if there are any systematic faunal changes through the Cerithium limestone Mb.

6. Conclusion

The Cerithium limestone Mb is a heterogenous bioturbated limestone made up of several carbonate microfacies with gradual or sharp boundaries that do not represent stratal bedding controlled by changes in the physical environment. The main microfacies include foraminiferal-dominated mudstone, foraminiferal-dominated bioclastic poor wackestone (10-25% bioclast content), with large amounts of ostracods and bivalve fragments and a bryozoan- and echinoderm-dominated bioclastic rich wackestone (25-50%) or packstone. Results show a minor vertical increase in bioclast content making the Cerithium limestone appear homogeneous on the macro sale. In contrast, the micro-scale shows a clear heterogeneity and many of

the microfacies boundaries within the thin sections can be linked to bioturbation traces. Therefore, the main cause of the microfacies distribution pattern at each site is likely due to bioturbation. Any large vertical changes in bioclast content between samples that could be linked to the *Thalassinoides* burrows are not visible. However, the micro-sized bioturbation traces visible within several samples point to micro scale heterogeneity being caused by the bioturbation of other unknown trace fossils. However, the degree of fragmentation and sorting through both units could indicate the presence of smaller water currents caused by gradient differences in the paleo bathymetry. The data do not support cyclicity or the presence of any major systematic changes in the energy regime, with only a minor bioclastic content increase being visible up section at Rødvig and not enough data points at Kulstirenden. More quantitative analysis of the sorting and fragmentation is needed for a concrete conclusion. The stratal thickness variation between the two studied sites was caused by condensation of the B subunit at Kulstirenden, an erosional hardground cutting through the Cerithium limestone Mb at different levels across Stevns Klint, and the uneven paleo-bathymetry due to the Højerup MB mounds. There are multiple differences between the units at Kulstirenden and Rødvig, with Kulstirenden having more of subunit A and less of subunit B. The B subunit is more condensed at Kulstirenden than at Rødvig but the reason for this cannot be determined with available data. The petrographic of subunit D shows a mudstone - bioclastic poor wackestone with a different faunal composition compared to the other units. The faunal composition of subunit D could indicate that the unit is a continuation of the Cerithium limestone Mb. However isotopic analysis and more quantitative analysis of the fauna of both localities are needed to confirm it.

7. References

Alegret, L., Thomas, E., & Lohmann, K. C. (2012). End-Cretaceous marine mass extinction not caused by productivity collapse. *Proceedings of the National Academy of Sciences*, *109*(3), 728-732. https://doi.org/10.1073/pnas.1110601109

Alvarez, L. W., Alvarez, W., Asaro, F., & Michel, H. V. (1980). Extraterrestrial cause for the cretaceous-tertiary extinction - experimental results and theoretical interpretation. *Science*, *208*(4448), 1095-1108. https://doi.org/10.1126/science.208.4448.1095

Andersen, C., Olsen, J. C., Michelsen, O., & Nygaard, E. (1982). Structural outline and development. *Danmarks Geologiske Undersøgelse Serie B*, *8*, 9-26. https://doi.org/10.34194/serieb.v8.7063

Anderskouv, K., Damholt, T., & Surlyk, F. (2007). Late Maastrichtian chalk mounds, Stevns Klint, Denmark - Combined physical and biogenic structures. *Sedimentary Geology*, *200*(1-2), 57-72. https://doi.org/10.1016/j.sedgeo.2007.03.005

Bernecker, M., & Weidlich, O. (2005). Azooxanthellate corals in the Late Maastrichtian - Early Paleocene of the Danish basin: bryozoan and coral mounds in a boreal shelf setting. In A. Freiwald & J. M. Roberts (Eds.), *Cold-Water Corals and Ecosystems* (pp. 3-25). Springer Berlin Heidelberg. https://doi.org/10.1007/3-540-27673-4_1

Boussaha, M., Thibault, N., Anderskouv, K., Moreau, J., & Stemmerik, L. (2017). Controls on upper Campanian-Maastrichtian chalk deposition in the eastern Danish Basin. *Sedimentology*, *64*(7), 1998-2030. https://doi.org/10.1111/sed.12386

Burnett, J. (1996). Nannofossils and Upper Cretaceous (sub-) stage boundaries–state of the art. *Journal of Nannoplankton Research*, *18*(1), 23-32.

Bralower, T. J., Cosmidis, J., Heaney, P. J., Kump, L. R., Morgan, J. V., Harper, D. T., Lyons, S. L., Freeman, K. H., Grice, K., Wendler, J. E., Zachos, J. C., Artemieva, N., Chen, S. A., Gulick, S. P. S., House, C. H., Jones, H. L., Lowery, C. M., Nims, C., Schaefer, B., . . . Vajda, V. (2020). Origin of a global carbonate layer deposited in the aftermath of the Cretaceous-Paleogene boundary impact. *Earth and Planetary Science Letters*, *548*, 116476. https://doi.org/10.1016/j.epsl.2020.116476

Desor, E. (1847). Sur le terrain danien, nouvel étage de la craie. *Bulletin de la Société géologique de France*, *4*(2), 179-182.

D'Hondt, S. (2005). Consequences of the cretaceous/paleogene mass extinction for marine ecosystems. *Annual Review of Ecology Evolution and Systematics*, *36*, 295-317. https://doi.org/10.1146/annurev.ecolsys.35.021103.105715

Flügel, E., & Munnecke, A. (2004). Microfacies of carbonate rocks: analysis, interpretation and application. *Springer Berlin, Heidelberg*. https://doi.org/10.1007/978-3-642-03796-2

Galehouse, J.S., 1971. Point counting. In: Carver, R.E. (Ed.), Procedures in Sedimentary Petrology: New York. John Wiley and Sons, pp. 385–407.

Gilleaudeau, G. J., Voegelin, A. R., Thibault, N., Moreau, J., Ullmann, C. V., Klaebe, R. M., Korte, C., & Frei, R. (2018). STable isotope records across the Cretaceous-Paleogene transition, Stevns Klint, Denmark: New insights from the chromium isotope system. *Geochimica Et Cosmochimica Acta*, *235*, 305-

332. https://doi.org/10.1016/j.gca.2018.04.028

Hansen, T. H., Clausen, O. R., & Andresen, K. J.. (2021). Thick- and thin-skinned basin inversion in the Danish Central Graben, North Sea – the role of deep evaporites and basement kinematics. *Solid Earth*, *12*(8), 1719–1747. https://doi.org/10.5194/se-12-1719-2021

Hansen, T., & Surlyk, F. (2014). Marine macrofossil communities in the uppermost Maastrichtian chalk of Stevns Klint, Denmark. *Palaeogeography Palaeoclimatology Palaeoecology*, *399*, 323-344. https://doi.org/10.1016/j.palaeo.2014.01.025

Hart, M. B., Feist, S. E., Hakansson, E., Heinberg, C., Price, G. D., Leng, M. J., & Watkinson, M. P. (2005). The Cretaceous-Palaeogene boundary succession at Stevns Klint, Denmark: Foraminifers and sTable isotope stratigraphy. *Palaeogeography Palaeoclimatology Palaeoecology*, *224*(1-3), 6-26. https://doi.org/10.1016/j.palaeo.2005.03.029

Hart, M. B., Feist, S. E., Price, G. D., & Leng, M. J. (2004). Reappraisal of the K–T boundary succession at Stevns Klint, Denmark. *Journal of the Geological Society*, *161*(5), 885-892. https://doi.org/doi:10.1144/0016-764903-071

Henehan, M. J., Ridgwell, A., Thomas, E., Zhang, S., Alegret, L., Schmidt, D. N., Rae, J. W. B., Witts, J. D., Landman, N. H., Greene, S. E., Huber, B. T., Super, J. R., Planavsky, N. J., & Hull, P. M. (2019). Rapid ocean acidification and protracted Earth system recovery followed the end-Cretaceous Chicxulub impact. *Proceedings of the National Academy of Sciences*, *116*(45), 22500-22504. https://doi.org/10.1073/pnas.1905989116

Heinberg, C. (1999). Lower Danian bivalves, Stevns Klint, Denmark: continuity across the K/T boundary. *Palaeogeography, Palaeoclimatology, Palaeoecology*, *154*(1-2), 87-106.

Ineson, J. R., Petersen, H. I., Andersen, C., Bjerager, M., Jakobsen, F. C., Kristensen, L., MØRK, F., & Sheldon, E. (2022). Early Cretaceous stratigraphic and basinal evolution of the Danish Central Graben: a review. *Bulletin of the Geological Society of Denmark*, *71*.

Leighton, A. D., Hart, M. B., & Smart, C. W. (2011). A preliminary investigation into calcareous dinoflagellate cysts and problematic microfossils from an expanded Cretaceous/Paleogene boundary section at Kulstirenden, Stevns Klint, Denmark. *Cretaceous Research*, *32*(5), 606-617. https://doi.org/10.1016/j.cretres.2011.05.011

Lowery, C. M., Bralower, T. J., Owens, J. D., Rodríguez-Tovar, F. J., Jones, H., Smit, J., Whalen, M. T., Claeys, P., Farley, K., & Gulick, S. P. (2018). Rapid recovery of life at ground zero of the end-Cretaceous mass extinction. *Nature*, *558*(7709), 288-291.

Lowery, C. M., Bown, P. R., Fraass, A. J., & Hull, P. M. (2020). Ecological Response of Plankton to Environmental Change: Thresholds for Extinction. *Annual Review of Earth and Planetary Sciences*, *48*(1), 403-429. https://doi.org/10.1146/annurev-earth-081619-052818

Lykke-Andersen, H., & Surlyk, F. (2004). The cretaceous-palaeogene boundary at Stevns Klint, Denmark: inversion tectonics or sea-floor topography? *Journal of the Geological Society*, *161*, 343-352. https://doi.org/10.1144/0016-764903-021

Machalski, M., & Heinberg, C. (2005). Evidence for ammonite survival into the Danian (Paleogene) from the Cerithium limestone at Stevns Klint, Denmark. *Bulletin of the Geological Society of Denmark*, *52*, 97-111. https://doi.org/10.37570/bgsd-2005-52-08

Myrow, P. M. (1995). Thalassinoides and the Enigma of Early Paleozoic Open-Framework Burrow Systems. *PALAIOS*, *10*(1), 58–74. https://doi.org/10.2307/3515007

Møller, J. J., & Rasmussen, E. S. (2003). Middle Jurassic – Early Cretaceous rifting of the Danish Central Graben. *Geological Survey of Denmark and Greenland Bulletin*, 1, 247-264. https://doi.org/10.34194/geusb.v1.4654

Nielsen, L. H. (2003). Late Triassic – Jurassic development of the Danish Basin and the Fennoscandian Border Zone, southern Scandinavia. *Geological Survey of Denmark and Greenland Bulletin*, *1*, 459-526. https://doi.org/10.34194/geusb.v1.4681

Nielsen, L., Boldreel, L. O., Hansen, T. M., Lykke-Andersen, H., Stemmerik, L., Surlyk, F., & Thybo, H. (2011). Integrated seismic analysis of the Chalk Group in eastern Denmark—Implications for estimates of maximum palaeo-burial in southwest Scandinavia. *Tectonophysics*, *511*(1-2), 14-26.

Patruno, S., Kombrink, H., & Archer, S. G. (2022). Cross-border stratigraphy of the Northern, Central and Southern North Sea: a comparative tectono-stratigraphic megasequence synthesis. *Geological Society, London, Special Publications*, *494*(1), 13-83. https://doi.org/doi:10.1144/SP494-2020-228

Perch-Nielsen, K. (1979). Calcareous nannofossil zonation at the Cretaceous/Tertiary boundary in Denmark. Proceedings, Cretaceous/Tertiary

Boundary Event Symposium, Copenhagen,

Rasmussen, J. A., Heinberg, C., & Hakansson, E. (2005). Planktonic foraminifers, biostratigraphy and the diachronous nature of the lowermost Danian Cerithium limestone at Stevns Klint, Denmark. *Bulletin of the Geological Society of Denmark*, *52*, 113-131. doi: 10.37570/bgsd-2005-52-09.

Rosenkrantz, A. 1937: Bemærkninger om det østsjællandske Daniens Stratigrafi og Tektonik. *Message from Geological society of Denmark*, 9(2), 199–212.

Rosenkrantz, A., Surlyk, F., Anderskouv, K., Frykman, P., Stemmerik, L., & Thibault, N. (2021). The K-T boundary strata north of Korsnæb, Stevns Klint, Denmark - evolution and geometry revealed in a long, horizontal profile. *Bulletin of the Geological Society of Denmark*, *69*. https://doi.org/10.37570/bgsd-2021-69-10

Schulte, P., Alegret, L., Arenillas, I., Arz, J. A., Barton, P. J., Bown, P. R., Bralower, T. J., Christeson, G. L., Claeys, P., Cockell, C. S., Collins, G. S., Deutsch, A., Goldin, T. J., Goto, K., Grajales-Nishimura, J. M., Grieve, R. A. F., Gulick, S. P. S., Johnson, K. R., Kiessling, W., . . . Willumsen, P. S. (2010). The Chicxulub Asteroid Impact and Mass Extinction at the Cretaceous-Paleogene Boundary. *Science*, *327*(5970), 1214-1218. https://doi.org/10.1126/science.1177265

Störling, T., Demangel, I., Lindskog, A., Andersson, J., Calner, M Conley, J. D., Richoz, S. (2024). A record of the K–P extinction aftermath: The Danish Cerithium Limestone. (Accepted for publication in *Bulletin of the Geological Society of Denmark*)

Surlyk, F. (1995). A cool-water carbonate ramp with bryozoan mounds: Late Cretaceous-Danian of the Danish basin. *Sepm Special Publication* [Cool-water carbonates]. Conference on Cool -Water Carbonates, Geelong, Australia.

Surlyk, F., Dons, T., Clausen, C.K. & Higham, J. 2003: Upper Cretaceous. In: Evans, D., Graham, C., Armour, A. & Bathurst, P. (eds): The Millennium Atlas: petroleum geology of the central and northern North Sea, 213–233. The Geological Society of London, London

Surlyk, F., Damholt, T., & Bjerager, M. (2006). Stevns Klint, Denmark: Uppermost Maastrichtian chalk, Cretaceous-Tertiary boundary, and lower Danian bryozoan mound complex. *Bulletin of the Geological Society of Denmark*, *54*, 1-48. https://doi.org/10.37570/bgsd-2006-54-01

Sørensen, K. (1986). Danish Basin subsidence by Triassic rifting on a lithosphere cooling background. *Nature*, *319*(6055), 660-663. https://doi.org/10.1038/319660a0

Thibault, N., Harlou, R., Schovsbo, N., Schioler, P., Minoletti, F., Galbrun, B., Lauridsen, B. W., Sheldon, E., Stemmerik, L., & Surlyk, F. (2012). Upper Campanian-Maastrichtian nannofossil biostratigraphy and high-resolution carbon-isotope stratigraphy of the Danish Basin: Towards a standard $\delta^{13}C$ curve for the Boreal Realm. *Cretaceous Research*, *33*(1), 72-90. https://doi.org/10.1016/j.cretres.2011.09.001

Thomsen, E. (1995). Kalk og kridt i den danske undergrund. In *Danmarks geologi fra Kridt til i dag* (Vol. 1, pp. 31-67). Geologisk Institut, Aarhus Universitet.

Vejbaek, O. V. (1989). Effects of asthenospheric heatflow in basin modeling exemplified with the danish basin. *Earth and Planetary Science Letters*, *95*(1-2), 97-114. https://doi.org/10.1016/0012-821x(89)90170-2

Wade, B. S., Pearson, P. N., Berggren, W. A., & Pälike, H. (2011). Review and revision of Cenozoic tropical planktonic foraminiferal biostratigraphy and calibration to the geomagnetic polarity and astronomical time scale. *Earth-Science Reviews*, *104*(1-3), 111-142.

Tidigare skrifter i serien ”Examensarbeten i Geologi vid Lunds universitet”:

639. Lodi, Giulia, 2022: A study of carbon, nitrogen, and biogenic silica concentrations in *Cyperus papyrus*, the sedge dominating the permanent swamp of the Okavango Delta, Botswana, Africa. (45 hp)
640. Nilsson, Sebastian, 2022: PFAS- En sammanfattning av ny forskning, med ett fokus på föroreningskällor, provtagning, analysmetoder och saneringsmetoder. (15 hp)
641. Jägfeldt, Hans, 2022: Molnens påverkan på jordens strålningsbalans och klimatsystem. (15 hp)
642. Sundberg, Melissa, 2022: Paleontologiska egenskaper och syreisotopsutveckling i borrkärnan Limhamn-2018: Kopplingar till klimatförändringar under yngre krita. (15 hp)
643. Bjermo, Tim, 2022: A re-investigation of hummocky moraine formed from ice sheet decay using geomorphological and sedimentological evidence in the Vomb area, southern Sweden. (45 hp)
644. Halvarsson, Ellinor, 2022: Structural investigation of ductile deformations across the Frontal Wedge south of Lake Vättern, southern Sweden. (45 hp)
645. Brakebusch, Linus, 2022: Record of the end-Triassic mass extinction in shallow marine carbonates: the Lorüns section (Austria). (45 hp)
646. Wahlquist, Per, 2023: Stratigraphy and palaeoenvironment of the early Jurassic volcaniclastic strata at Djupadalsmölla, central Skåne, Sweden. (45 hp)
647. Gebremedhin, G. Gebreselassie, 2023: U-Pb geochronology of brittle deformation using LA-ICP-MS imaging on calcite veins. (45 hp)
648. Mroczek, Robert, 2023: Petrography of impactites from the Dellen impact structure, Sweden. (45 hp)
649. Gunnarsson, Niklas, 2023: Upper Ordovician stratigraphy of the Stora Sutarve core (Gotland, Sweden) and an assessment of the Hirnantian Isotope Carbon Excursion (HICE) in high-resolution. (45 hp)
650. Cordes, Beatrix, 2023: Vilken ny kunskap ger aDNA-analyser om vegetationsutvecklingen i Nordeuropa under och efter Weichsel-istiden? (15 hp)
651. Bonnevier Wallstedt, Ida, 2023: Palaeocolour, skin anatomy and taphonomy of a soft-tissue ichthyosaur (Reptilia, Ichthyopterygia) from the Toarcian (Lower Jurassic) of Luxembourg. (45 hp)
652. Kryffin, Isidora, 2023: Exceptionally preserved fish eyes from the Eocene Fur Formation of Denmark – implications for palaeobiology, palaeoecology and taphonomy. (45 hp)
653. Andersson, Jacob, 2023: Nedslagskratrars inverkan på Mars yt-datering. En undersökning av Mars främsta ytdateringsmetod ”Crater Counting". (15 hp)
654. Sundberg, Melissa, 2023: A study in ink – the morphology, taphonomy and phylogeny of squid-like cephalopods from the Jurassic Posidonia Shale of Germany and the first record of a loligosepiid gill. (45 hp)
655. Häggblom, Joanna, 2023: En patologisk sjölilja från silur på Gotland, Sverige. (15 hp)
656. Bergström, Tim, 2023: Hur gammal är jordens inre kärna? (15 hp)
657. Bollmark, Viveka, 2023: Ca isotope, oceanic anoxic events and the calcareous nannoplankton. (15 hp)
658. Madsen, Ariella, 2023: Polycykliska aromatiska kolväten i Hanöbuktens kustnära sediment - En sedimentologisk undersökning av vikar i närhet av pappersbruk. (15 hp)
659. Wangritthikraikul, Kannika, 2023: Holocene Environmental History of Warming Land, Northern Greenland: a study based on lake sediments. (45 hp)
660. Kurop, Anna, 2023: Reconstruction of the glacier dynamics and Holocene chronology of retreat of Helagsglaciären in Central Sweden. (45 hp)
661. Frisendahl, Kajsa, 2023: Holocene environmental history of Washington Land, NW Greenland: a study based on lake sediments. (45 hp)
662. Ryan, Cathal, 2023: Luminescence dating of the late Quaternary loess-palaeosol sequence at Velika Vrbica, Serbia. (45 hp)
663. Lindow, Wilma, 2023: U-Pb datering av zirkon i metasediment tillhörande Stora Le-Marstrand, SV Sverige. (15 hp)
664. Bengtsson, Kaisa, 2023: Geologisk karaktärisering av den kambriska Faluddensandstenen i Östersjön och dess lämplighet för koldioxidlagring. (15 hp)
665. Granbom, Johanna, 2023: Insights into simple crater formation: The Hummeln impact structure (Småland, Sweden). (45 hp)
666. Jonsson, Axel, 2023: Datering av vulkanen Rangitoto, Nya Zeeland, genom paleomagnetiska analysmetoder. (15 hp)
667. Muller, Elsa, 2023: Response of foraminifera *Ammonia confertitesta* (T6) to ocean acidification, warming, and Deoxygenation An experimental approach. (45

hp)

668. Struzynska, Patrycja, 2023: Petrography, geochemistry, and origin of deep magmatic cumulates in the Canary Islands – the xenolith record. (45 hp)
669. Krätzer, Tobias, 2023: Artificiella torskrev i Hanöbukten: Förstudie. (15 hp)
670. Khorshidian, Farid, 2023: 3D modelling and resistivity measurements for hydrogeological assessments in the northern part of Vombsänkan. (45 hp)
671. Sundberg, Oskar, 2023: Methodology for Stored Heat "Heat In Place" (HIP) assessment of geothermal aquifers – Exemplified by a study of the Arnager Greensand in SW Scania. (45 hp)
672. Haraldsson, Emil, 2023: Kan akademin hjälpa industrin utveckla mer robusta grundvattenmodeller? En studie av moderna Svenska industriframtagna grundvattenmodeller. (15 hp)
673. Barabas, Ricky, 2024: Kan chockmetamorfos i okonventionella mineral hjälpa till att identifiera nedslagskratrar? (15 hp)
674. Nilsson, Sebastian, 2024: The glaciotectonic evolution of Ven, Sweden: insights from a comprehensive structural, sedimentological, and geomorphological analysis. (45 hp)
675. Brotzen, Olga M., 2024: A new Lagerstätte-like fossil assemblage from the early Silurian of Mösseberg, Sweden. (45 hp)
676. Eng, Simon, 2024: Precursors to the South Atlantic Anomaly - Magnetic field variations in Lake Eilandvlei, South Africa. (45 hp)
677. Husén, Simon, 2024: Structural Geological Model of the Kaunisvaara Mining District, Norrbotten, Sweden. (45 hp)
678. Hjalmarsson, Tilda, 2024: Det underkambriska problematiska fossilet *Spatangopsis* - Vad är dess verkliga affinitet? (15 hp)
679. Kuberna, Marcos, 2024: En litteraturstudie om klorparaffiner i grundvattnet och dess implikationer på hälsa och miljö. (15 hp)
680. Persson, Viktor, 2024: Litteraturstudie: HIMU ursprung och framtid. (15 hp)
681. Selin, Sigrid, 2024: Hur kan paleoekologiska studier hjälpa oss att bättre förstå hur de ekosystem vi anser skyddsvärda har formats och hur de bör vårdas? (15 hp)
682. Rey, August, 2024: Isrörelser och havstransgressioner speglade i Kåsebergåsen. (15 hp)
683. von Vultée, Anton, 2024: Babets kvarlevor - En morfologisk och sedimentologisk undersökning av överspolningssediment vid Tobisvik, Simrishamn. (15 hp)
684. Olsson Roso, Céline, 2024: Fåglarnas ursprung och tidiga utveckling. (15 hp)
685. Nawrocki, Bartosz, 2024: Karaktärisering av Cr-spinell i den ordoviciska Lokaformationen vid Skultorps stenbrott, Billingen. (15 hp)
686. Rydh, Alexander, 2024: Unraveling Magnetic Anomalies: A Study of Earth's Field Asymmetries during the Laschamps Excursion. (15 hp)
687. Svensson, Ludvig, 2024: Echoes of impact: A petrographic analysis and classification of impact breccias from Hummeln, Sweden. (15 hp)
688. Pålsson, Malin, 2024: Detektion av utsläppsplymer med avancerat ekolod – Undersökning av utsläpp av avloppsvatten från pappersbruk i havet med EK80, CTD & filmmaterial. (15hp)
689. Ivanovic, Edwin, 2024: Går det att se echinodermernas utveckling och diversifiering under ordovicium i tunnslip? (15 hp)
690. Blomvall, Marlene, 2024: Analys av morfologi, beteende och tafonomi hos ett exceptionellt bevarat fågelfossil från Furformationen (eocen), Danmark . (15 hp)
691. Elfström, Dari, 2024; Geomorfologisk studie av Jezerokraterns kant (Mars): Potentiella mekanismer bakom kraterkantens nuvarande utseende. (15 hp)
692. Andersson, Jacob, 2024: The Cerithium limestone Member at Stevns Klint reflecting the carbonate production recovery after the K/Pg mass-extinction. (45 hp)

LUNDS UNIVERSITET

Geologiska institutionen
Lunds universitet
Sölvegatan 12, 223 62 Lund